Interaction between the thermohaline circulation and sea ice in Dansgaard-Oeschger cycles.

Dirk van der Veek supervisors: R.S.W. van de Wal & A.S. von der Heijdt

Abstract:

During the last glacial period large fluctuations on a millennial timescale are observed in the Northern Hemisphere. Several mechanisms have been proposed to explain these Dansgaard-Oeschger (DO) cycles. The most commonly accepted mechanism is related to oscillations in the Atlantic meridional overturning circulation (AMOC), brought about by periodic changes in the freshwater flux into the North Atlantic. In a more recent theory it is proposed that the dominant process is subsurface warming in the Nordic Seas induced by increasing sea ice cover, which eventually leads to instability of the water column. Both of these theories correspond well to part of the observations, but neither are unable to explain the full range of observational data. Here we combine both mechanisms in a conceptual model study. In addition we include a land ice component to capture the effect of Heinrich events. It is shown that the model results correspond well to observational data and that the combination of these mechanisms is able to explain more of the features of the DO-cycle than each of the individual mechanisms. The full conceptual model provides an explanation for the structure of the events and accounts for the duration of stadials and interstadials and the variability therein. It shows why Heinrich events are triggered during stadials and how they can delay the occurrence of a subsequent DO-event. As a consequence it also explains one of the most striking features of the DO-cycle; the double peak in the probability distribution of the waiting time between consecutive events.

Contents

1 Introduction

During the last glacial period the climate of the north Atlantic region was far from stable. The reconstruction of the temperature over Greenland, based on the analysis of oxygen isotopes from ice cores, reveals a pattern of rapid warming (5-10°C in a few decades) proceeded by a more gradual cooling (Dansgaard et al., 1984; Johnsen & Dansgaard, 1992; Bond, 1993; Dansgaard, 1993). This pattern, that has come to be known as the Dansgaard-Oeschger (DO) cycle, has puzzled paleoclimatologists ever since its discovery.

The most commonly accepted explanation for these fluctuations relies on periodic changes in the Atlantic meridional overturning circulation (AMOC). In simple models describing the AMOC the system appears to be bimodal. There is a warm interstadial mode in which the circulation patterns are similar to those observed today and a stadial mode, which is marked by severely reduced circulation. Under glacial conditions the stadial mode is stable and the interstadial mode marginally unstable. Nonetheless variations in the freshwater flux into the north Atlantic can temporarily push the system from the stable cold mode to the warm interstadial mode. This takes place when the fresh water flux drops below a threshold value, the system then suddenly jumps to the mode with stronger circulation. This causes sudden warming events at high latitudes, as more energy is transported to the northern parts of the Atlantic. After these events the freshwater flux will increase again due to the higher melt rate caused by the higher temperatures. This in turn will slow down the AMOC due to the reduction of deepwater formation at high latitudes. Hence the temperatures drop again and this will eventually lead to the system switching back to the cold mode (Ganopolski & Rahmstorf, 2001).

Sea ice cover variations play a dominant role in another physical mechanism proposed to be at the root of the cycle. According to this theory the sea ice acts as an insulating blanket covering the ocean. The ocean below this layer warms because it still has an energy influx from lower latitudes but has lost part of its ability to release heat. The sea ice is shielded from the warming ocean below by a fresh water layer directly below it. The warming of the ocean at mid depth will decrease the density and eventually this will lead to destabilization of the water column, at which point the energy stored in the ocean will suddenly be released and cause the rapid warming (Rasmussen & Thomsen, 2004; Dokken et al., 2013; Singh, 2013).

Many models have been created that are capable of producing a signal that captures the basic structure of a DO-event, but no consensus has been reached on which of these models delivers the best description of the actual physics underlying the DO-cycle. To discriminate between the models Greenland ice core data alone does not suffice, as one temperature signal simply doesn't give enough information about the physics that caused the variations. However since its discovery DO-cycles have been found in many other indicators of past climate. Imprints of the cycle have been found in stalagmite proxy records all over Eurasia (Wang et al., 2001; Spötl and Mangini, 2002; Fleitmann et al., 2009) and as far from Greenland as is possible; in the temperature reconstructions of Antarctica (EPICA community members, 2006). In addition it has been suggested that there is a link between the DO-cycle and the massive ice berg discharges known as Heinrich events. Perhaps less surprising, but probably more relevant for unraveling the physics, the DO-cycle was also found in ocean temperature reconstructions of the north Atlantic. Below the Iceland-Scotland ridge the temperature closely follows that of the Greenland ice cores (Bond, 1993). However above this ridge the ocean temperatures show contrasting changes; temperatures were 2-8° higher during the stadials than during the interstadials (Rasmussen & Thomsen, 2004). All this data has been linked to the DO-cycles and provides more information about what exactly happened during DO-events. This means that there are more phenomena for which any model describing this cycle should provide an explanation, and this in turn makes it easier to discriminate between the multitudes of models that have been proposed so far.

Against this background this thesis will proceed as follows: The next chapter will give an overview of all the observational data. Paragraph 2.1 will present an analysis of the patterns in the actual signal, and paragraph 2.2 will present related observational data, such as Heinrich events and ocean temperature reconstructions for the same period. Paragraph 2.3 formulates a synthesis and provides a summary of all patterns that any conceptual model describing the DO-cycle should ideally account for. Chapter 3 provides an overview of the models that have been proposed so far and an analysis of to what extent they can explain the key characteristics of the pattern. Chapter 4 presents my own model, the results of which will be presented in chapter 5. Chapter 6 provides a discussion of the results, and a summary of the conclusions is given in chapter 7.

2 Observations

2.1 Analysis of the ice core data

Thorough analysis of the Greenland isotope data can provide valuable insights into the underlying physical mechanism reflected in the observations. Figure 1 shows the $\delta^{18}O$ signal from the GISP2 ice core, the numbers indicate the 20 classical DO-events. Almost all the DO-events have the same basic structure: stadial conditions are terminated when a sudden rapid warming event pushes the system to interstadial conditions. The interstadial is marked by a gradual temperature decrease, until in another sudden jump the system moves back to stadial conditions. This pattern can most clearly be observed in DO-events 19 and 20, but the other events have roughly the same structure. The main difference between the separate events is the durations of the stadials and interstadials.

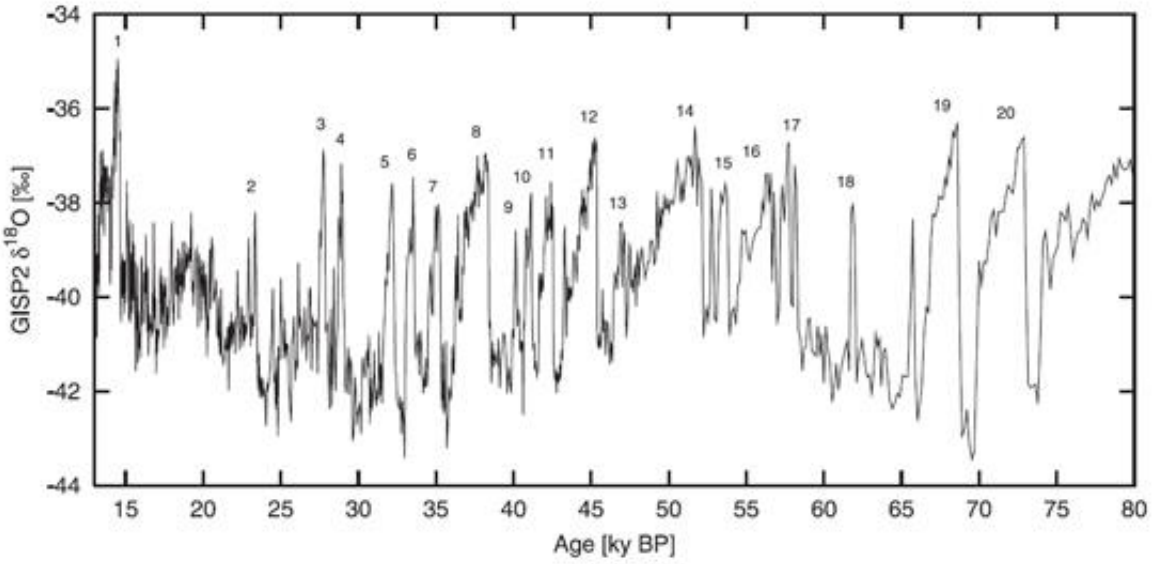

Figure 1, Oxygen isotop ($\delta^{18}O$) recored from Greenland (GISP ice core[Grootes and Stuiver, 1997]). Numbers above $\delta^{18}O$ maxima denote the classical DO-events [Johnsen et al., 1992; Dansgaard et al., 1993]. (From Schulz, 2002).

The main explanation of the basic structure of the signal is that glacial climate is a bimodal system, that is to say that it has two stable equilibria. The oscillations are caused by shifts between these different modes. Rapid warmings occur when the system jumps from its cold stadial mode to the warm interstadial mode (Dansgaard et al., 1982; Oeschger et al., 1984; Broecker et al., 1985). Because the interstadial mode is not fully stable immediately after the jump the temperatures gradually decrease, this is then followed after a while by another sudden jump back to the stadial conditions. An alternative explanation is that the dynamics are not that of a bimodal system, but that it is caused by an autonomous irregular oscillation in the climate system. This means that there are no stable equilibrium states, but one equilibrium trajectory through the parameter space. As the system follows this trajectory it moves through its different states, resulting in the oscillation in the temperature. The irregularity of the oscillation could be the result of the “noise” in the system.

2.1.1 Time spacing

The hypothesis that the glacial climate is a bimodal system doesn't provide explicit information about the physics that underlie the oscillations, nonetheless it gives a direction to the process of unraveling the dynamics of the system. Braun (2011) investigated the probability that the shifts between the different modes are merely caused by random perturbations. The one parameter stochastic process, in which DO-events are triggered every time a random forcing crosses a fixed threshold, could be statistically rejected. The reason for this is that waiting time between two consecutive events is minimally about a thousand years and the probability peaks around 1500 years. For the one parameter process however the probability is highest for waiting times of 0 years and decreases exponentially with increasing waiting time. A two parameter process, in which the threshold value has a certain relaxation time, could not be rejected a priori. Braun didn't propose randomly triggered excursions as a mechanism explaining the DO-cycle, but did suggest that a two parameter process should be used in favor of the one parameter process as a null hypothesis for testing the probability of proposed mechanisms against randomly triggered events.

The main argument against randomly triggered events is that spectral analysis showed that there is a dominant frequency of 1/1470 years in the signal (Grootes and Stuiver, 1997). This suggests that there is an as of yet undiscovered cycle with a period of 1470 years in the climate system. This cycle has been proposed to be of solar origin, internal to the AMOC or even in the meridional fresh water flux. Even though there is a significant spectral peak at 1/1470 year, this does not necessarily mean that this frequency is present over the whole domain of the signal. The signal could very well be non-stationary, as there is no a priori reason to assume that it isn't. Indeed Schulz (2002) showed that the spectral peak is to a great extent caused by DO-events 5-7, and that when these three events are removed from the data the significant peak disappears almost entirely.

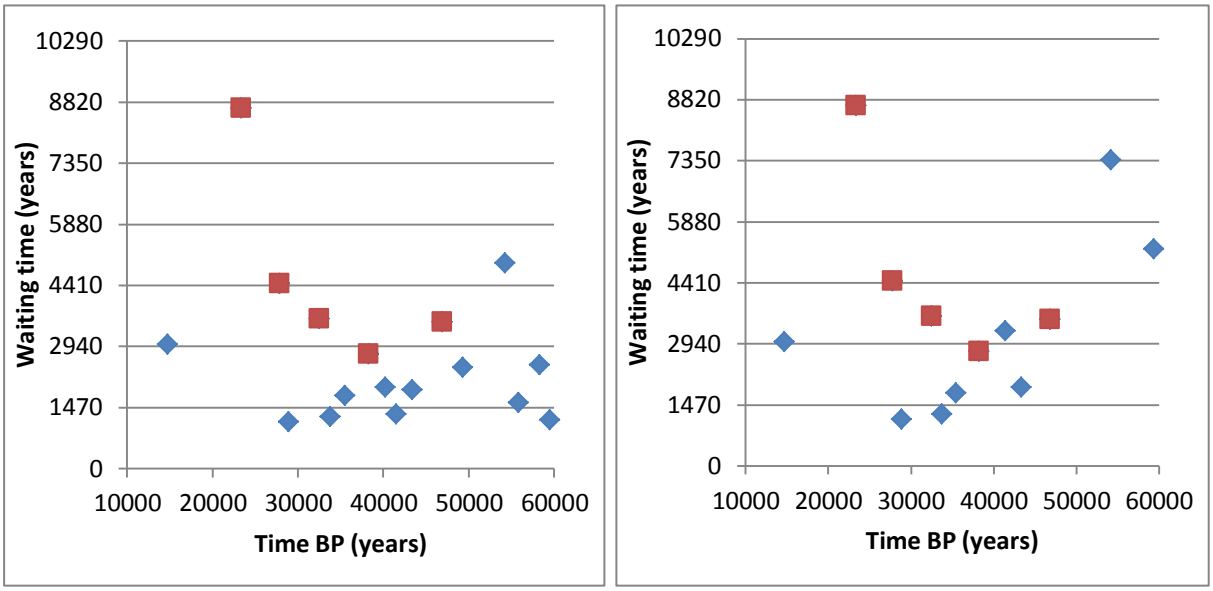

Figure 2, Waiting time between consecutive DO-events vs. time before present. Timing of the events is based on the analysis of Ditlevsen et al. (2007). The panel A uses the classical DO-events, panel B the canonical DO-events (chosen with the selection criteria of Schulz (2002). The red squares indicate which periods between DO events were also marked by Heinrich events.

In spite of this Schulz then proceeds to show that the waiting time between consecutive DO-events is in almost all cases within a 20% distance from either 1470 year nor a multitude thereof. To arrive at this conclusion Schulz needed to apply new selection criteria to filter the DO-events and arrive at his so called "canonical DO-event". Four of the classical DO-event are not taken into account, and one

warming event that is not seen as a classical DO-event is added. If selected in this manner the waiting time does seem to have a preference for multiples of 1470 year, and this is presented as an argument in favor of the 1470 year cycle.

The basic idea is that the cycle is so subtle that it does not necessarily trigger DO-events. However during one phase of the cycle the system is closer to a threshold and thus random noise can tip the system more easily towards its other equilibrium. During the phase when the system is far from the threshold this is highly improbable, so no DO-events occur. This leads to a probability distribution of the waiting time between DO-events that shows peaks around 1470 and multiples thereof. Figure 2 shows an analysis similar to that of Schulz for both the classical DO-events (panel a) and his canonical DO-events (panel b). The horizontal lines are the multiples of 1470 year, so according to Schulz's theory the waiting times should group in the proximity of these lines. For the classical DO-events this does not appear to happen at all, but for the canonical DO-events it may be observed, although if we apply the timing of the events proposed by Ditlevsen (2007) it is less obvious than in the original paper by Schulz.

Looking at the classical DO-events in panel A of figure 2, it is interesting to note that the longer waiting times between DO-events tend to be accompanied by Heinrich events. It is well known that these ice berg discharges counter intuitively take place during long stadials and it therefore has been proposed that Heinrich- and DO-events are related (Bond, 1993).

2.1.2 Early warning signals

Another way of extricating information about the dynamics from the temperature reconstruction is to investigate whether or not there are detectable early warning signals prior to DO-events. A bimodal system can switch to another mode when an external forcing crosses a certain threshold, such thresholds are called "tipping points". In general systems approaching a tipping point show a decrease in their variability, implying that the autocorrelation increases. This increase in autocorrelation is referred to as an early warning signal (EWS), as it is an indication that the system might go through an abrupt transition in the near future (see e.g. Held and Kleinen, 2004; Livina and Lenton, 2007; Scheffer et al., 2009; Ditlevsen and Johnsen, 2010).

If such EWS's are present in the ice core signal prior to DO-events, this can be seen as an indication that these fluctuations are indeed caused by the dynamics of a bimodal. Ditlevsen and Johnsen (2010) concluded that there were no significant detectable EWS's before the DO-events. Cimatoribus (2013) came to contrasting conclusions because he did find weak EWS's when he examined the ensemble of events. Hence the findings of Cimatoribus favor bimodal dynamics, in which the system switches between two different climate equilibrium states in response to a changing external forcing (note; "external" should be read here in the mathematical sense, as external to the system considered, it does not necessarily mean external to the climate system), which either forces the transition directly or paces it through stochastic resonance. These findings are however not convincing enough to really rule out any of the other possible mechanisms, such as autonomous oscillations.

One of the main problems with such analysis is that one has to assume that the noise in the system is independent of the state of the system. The noise in these simple models represents processes that take place on timescales much shorter than the timescales concerned. Under certain circumstances these can indeed be represented in a satisfactory fashion by noise, nonetheless the assumption that these processes are unaffected by the state of the system is often not robust. To give an example a study by Li (2005) showed that the temperature over Greenland was significantly influenced by the

sea ice extent, however besides influencing the temperature itself sea ice cover variations could also influence the autocorrelation of the temperature signal. If there is no sea ice present then surface air temperatures are to large extent influenced by the temperature of the ocean, whereas coupling between atmosphere and ocean is weaker when there is a lot of sea ice. As ocean temperature anomalies in general have longer life spans than those in the atmosphere the autocorrelation of the air temperature could be strongly affected by the sea ice cover variations. This is just one example of a mechanism through which the state of the system can influence the processes that lead to the "noise", and can thus affect the pattern in the "noise". In general one has to be careful with the assumption of state independent noise, and without this assumption it is impossible to draw firm conclusions from this sort of analysis.

2.2 Related observations

Since the initial discovery of the DO-cycle, observational studies have shown that this oscillation left its imprint in almost the entire northern hemisphere (Rahmstorf, 2002; Voelker, 2002). Greenland stadials are coincident with wetter and warmer conditions in Europe (Genty et al., 2003), and with aridity in the southwestern parts of North America (Wagner et al., 2010). It has even been shown to affect the Indian summer monsoon (Schulz et al., 1998; Pausata et al., 2011). Although these observations are interesting it is hard to decide whether they are cause or consequence of the DO-events. Climate model studies indicate that DO-events in the north Atlantic can indeed have a global effect (e.g. Wang et al., 2001; Garcin et al., 2006; Harrison and Sánchez-Goñi, 2010).

But the influence of the DO-cycle is not even limited to the northern hemisphere, as mentioned it is also present in the reconstructions of the temperature of Antarctica. The signal in the ice cores show a one to one correspondence to the DO-events, but the changes are out of phase. It has been shown that magnitude of the temperature rise in Antarctica is very well correlated to the duration of the corresponding DO-stadial (EPICA community members, 2006). This indicates that the two are connected, probably by the AMOC. It can easily be understood how reduction of the AMOC leads to warming of the southern ocean by considering the situation at the equator. Close to the surface warm water is transported northwards, whereas at depth colder water is transported southwards. This means that the AMOC causes a net cooling of the southern oceans, and thus a reduction of the AMOC can cause warming on Antarctica (Crowley, 1992; Broecker, 1998; Stocker & Johnsen, 2003; Knutti, 2004). To get more insight into the changes in the AMOC and how this affected the ocean temperatures the next section will provide an overview of the relevant observations.

2.2.1 Ocean temperature reconstructions

The first observations linking the DO-cycle to changes in the surrounding ocean were sea surface temperature reconstructions from sediment cores in the North Atlantic (Bond, 1993). These cores were located south of the Iceland Scotland ridge and showed a pattern that closely matched that of the Greenland ice cores. It was these records that established the link between the DO-oscillation and Heinrich events. Based on the ocean data the DO-events can be bundled in series of gradually cooler interstadials, which are followed by a relatively long stadial during which a Heinrich event occurs. When this stadial is finally terminated it is followed by a strongly pronounced interstadial which marks the beginning of a new Bond-cycle. Even thought the connection does not explain whether long stadials cause Heinrich events or vice versa, it is nonetheless a clear indication that ice sheets need to be included in the dynamics to understand the full variability of DO-cycles and Heinrich events.

As the sea surface temperature reconstructions from the North Atlantic follow the pattern of the ice cores this is in good agreement with the theory that the DO-cycle is caused by changes in the AMOC. Measurements north of the Iceland-Scotland ridge (referred to as the Nordic Seas) however prove harder to reconcile, as they show a distinctly different pattern; temperatures were significantly higher during the stadials. The increased temperature in intermediate depth water appeared to be 2-4° during normal stadials, and up to double that during the Heinrich stadials (Rasmussen &Thomsen, 2004). This paradoxal warming of the ocean in the cold mode can't be explained by the suppressed AMOC. Another mechanism needs to be involved and it is likely that it has to do with variations in sea ice cover. During the stadials the sea ice will extend further south, possibly covering a large part of the Nordic Seas. The sea ice has an insulating effect and together with a fresh water layer that shields the ice from the ocean below it, it can drastically reduce the capacity of the ocean to release heat into the atmosphere. This means that if there is significant heat transport into the sea ice covered part of the ocean by the AMOC, this will inevitably lead to a warming of the water below the ice.

Dokken (2013) analyzed a greater number of sediment cores taken from the Nordic Seas and on the Iceland-Scotland ridge. This data further supports the idea that during the interstadials the conditions in the Nordic Seas were quite similar to those observed today. During stadials however it almost fully ice covered, with a fresh surface layer directly below the sea ice. So the general pattern appears similar to that found by Rasmussen & Thomsen, but his interpretation of the data is slightly different. Dokken states that in the two modes there are different mechanisms leading to deepwater formation. During the interstadials there is deep open ocean convection, but during stadials when this becomes impossible due to extensive sea ice cover there is still some deep water production through sinking of the dense brines formed along the Scandinavian coast. Part of the isotope signal that led Rasmussen & Thomsen to the conclusion that the warming in the intermediate waters was 2-8° could be caused by injection of these dense brines into the intermediate layers. The influence of this dense isotopically light water could account for a part of the signal, he therefore concludes that the range suggested by Rasmussen & Thomsen is probably an overestimation. Nonetheless the temperature at intermediate depth did definitively increase during the stadials.

2.2.2 Heinrich events

In the North Atlantic sediment cores layers have been found with significantly increased ice rafted detritus (IRD) (Heinrich, 1988). These layers indicate that on several occasions during the last glacial period phases of massive ice berg discharges took place. Six of these so called Heinrich events punctuated the last glacial period, all of them took place during longer than average DO-stadials. Various mechanisms have been proposed to cause these ice discharges, but all are somehow related to instabilities of the Laurentide ice sheet. These instabilities likely occur because of the non linear dynamics associated with alterations of basal conditions caused by changes in the flow (MacAyeal, 1993; Calov et al., 2002). These instabilities could also be triggered by ice shelf collapses, either due to changes in the atmosphere (Hulbe et al., 2004), tidal effects (Arbic et al., 2004), or warming of the subsurface water (Alvarez Solas, 2011). The freshwater flux associated with Heinrich events has been suggested to disrupt the AMOC by preventing North Atlantic deep water (NADW) formation. The severe reduction of the AMOC is then in turn supposed to lead to the elongated the DO-stadials. There is indeed evidence that the AMOC was strongly reduced during the Heinrich events (Sarnthein et al., 1994). And this is further supported by the relatively large warming in Antarctica during Heinrich events. However recent data has revealed that the peaks in IRD associated with Heinrich events occur several hundred years after the onset of the stadial (Hall, 2006; Hemming, 2004). These observations are hard to reconcile with the theory that the freshwater flux was responsible for the reduction of the AMOC that supposedly was the cause of the stadial conditions.

Closer examination of the sediment layers associated with the Heinrich events, revealed that the initial increase in IRD is of Scandinavian origin (Hemming, 2004). It has been suggested that this relatively small event prior to the actual instability of the Laurentide ice sheet could have contributed to the initiation of the AMOC reduction (Hall et al., 2006). It could also be directly involved in the collapse of the ice shelves connected to the Laurentide ice sheet, either through sea-level rise (Levermann et al., 2005) or subsurface temperature increase (Mignot et al., 2007). Removal of these ice shelves could lead to substantial acceleration of the ice-streams and an increase in the ice berg discharge, this then would be the onset of the actual Heinrich event (Alvarez-Solaset al., 2010b; Hulbe, 2010; Shaffer et al., 2004).

2.3 synthesis

The most common explanation for the DO-cycle concerns switches in AMOC between two different modes of operation. These jumps between the two equilibriums of the system are supposed to be brought about by variations in the freshwater flux into the North Atlantic. Although there is indeed convincing evidence linking the DO-cycle to changes in the AMOC, it is less obvious whether or not these changes were really triggered by changes in the freshwater flux. It has been shown that the Heinrich events occur after the AMOC had already slowed down, or had even collapsed. Furthermore for most DO-stadials there are no significant increases in the IRD have been found in Atlantic sediments. This means that the ice berg calving rates were not significantly different and that variations in the freshwater flux on the DO-time scales was probably not caused by ice sheet instabilities. The meridional water flux through the atmosphere has been proposed as another mechanism to create the freshwater anomalies this theory builds upon, but whether there really are significant changes in this flux on DO-timescales remains invalidated.

Another observation that is hard to explain relying solely on changes in the AMOC is the warming of the intermediate depth waters in the Nordic Seas. This observation has in turn been used as an argument in favor of a mechanism based on variations in sea ice extent. In this theory the sea ice expansion during stadials increasingly insulates the ocean and causes the subsurface waters to warm, eventually leading to instability of the water column and the sudden release of the energy.

As both theories have observations that support them and others that they leave unexplained, the way forward may be to combine the positive aspects of both and focus on integrating these alternatives into one theory that accounts for all the observations. As there is undeniable evidence for changes in the AMOC this will certainly have to be included. Changes in the AMOC can be brought about in various ways. Wind driven upwelling in the Southern ocean might significantly influence the AMOC (Toggweiler & Samuels, 1993), but the relative importance of this with respect to the THC is still under discussion (for example; Rahmsdorf, 1997). A model study by Delworth (2008) showed that it takes relatively large changes in the atmospheric circulation to bring about significant changes in the AMOC (for example: a 2° poleward shift in the windpattern causes a 2 Sv change in the AMOC after 200 years), especially on short time scales.

On the timescale of the DO-cycle changes in the AMOC are most likely brought about by thermohaline effects. The focus has been on the freshwater flux into the north Atlantic as the driver behind changes in the THC, however this not the only physical mechanism that can bring about such changes. The warming of the subsurface water in Nordic Seas could also be a contributing factor. The THC is driven by the density difference between the waters near the North and South Pole, the bigger the density difference the stronger the circulation. Under normal circumstances a decreasing density in the North Atlantic decreases the density difference between the polar waters, as a consequence this leads to suppression of the THC.

This means that warming of the subsurface waters in the Nordic Seas would act to suppress the THC. The THC would remain suppressed until the subsurface water temperatures decrease again. In this case the cooling is brought about by the sudden increase in the vertical mixing caused by the eventual instability of the water column during the DO-event. This would mean that the AMOC would strengthen almost immediately after a DO-event, which in turn would further strengthen the warming.

As ice sheet instabilities that lead to Heinrich events are likely triggered by increased melt rates, it is hard to explain why these would occur during stadials relying solely on freshwater driven changes in AMOC. However when we include the subsurface warming as a critical aspect of the DO-cycle this would be a plausible trigger for ice sheet instability. Because warming of the mid-depth ocean would mean that the melt rates at the bottom of the shelves would increase during stadials. From the sediment records it becomes clear that there are precursor events with increased IRD deposits from Scandinavian origin, these could be caused directly by increased melt rates at the bottom of Scandinavian outlet glaciers/ice shelves due to subsurface warming in the Nordic Seas. In turn this discharge of freshwater would lead to a strengthening of the halocline and a suppression of the AMOC, both of which act to postpone the instability of the water column in the Nordic Seas. The strengthening of the halocline would allow the subsurface waters to warm even further before the DO-event is triggered. Sea level changes in the Hudson bay area could then possibly, in combination with increased subsurface warming thereafter trigger the instabilities in the Laurentide ice sheet.

3 Model studies

Since the discovery of the DO-cycle many models have been created that are capable generating a signal similar to that of the Greenland ice cores, however the discussion about which of these models represents the true physics of the DO-oscillation is still open. Based on the dynamics the models can roughly be divided into two types: the bimodal systems in which a changing external forcing causes the system to shift between two climate modes, and the autonomous oscillations. Not all models can be treated here, as there are far too many. A selection is presented of models that are interesting by themselves, and represent a class of models, such that all together they provide an overview of the spectrum of physical mechanisms.

3.1 Systems with external forcing

An insightful investigation into dynamics of the AMOC is given by Ganopolski and Rahmstorf (2001). Using the CLIMBER-2 model they show that the AMOC does indeed appear to have two modes of operation, one "warm" mode with strong (northward) North Atlantic deep water (NADW) formation, and one "cold" mode with reduced (and more southward) NADW formation and related northward heat flux. The fresh water flux into the North Atlantic acts as the most important control parameter, that can cause shifts between the modes.

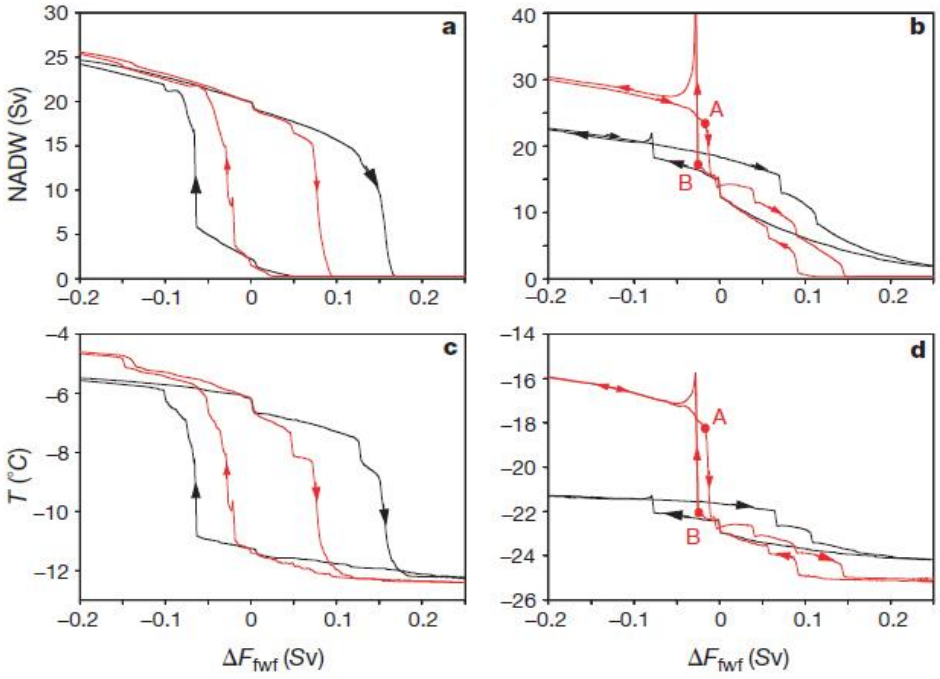

Figure 3, Stability diagrams for the Atlantic thermohaline circulation in the coupled model. The present climate (left panels) differs substantially from the glacial climate (right panels). To calculate the stability diagram the method of Rahmstorf (1995) was used. The freshwater perturbation ΔF_{fwf} was added in the latitude belt 20-50 °N to obtain the black curves, and in the latitude belt 50-70°N to obtain the red curves. Panels a and b show the ocean circulation response to the freshwater input (in terms of the maximum value of the Atlantic stream function, labeled NADW for North Atlantic Deep Water flow, while panels c and d show the North Atlantic sector air temperature (60-70° N). (From Ganopolski and Rahmstorf (2001))

Figure 3 shows the stability diagrams of the AMOC with respect to the freshwater flux into certain latitude bands (20-50 °N to attain the black curves and 50-70 °N to attain the red curves) for the current climate (left panels) and glacial conditions (right panels). As many studies have already indicated under current climate conditions the overturning circulation shows a clear hysteresis loop, as the strength of the circulation itself is of influence on the magnitude of freshwater flux that is needed for the system to shift to the other mode. The hysteresis loop is narrower when the freshwater is injected directly into the latitude of the Nordic seas, as this is where the NADW formation takes place. When freshwater flux is added to the ocean on lower latitudes this has a less direct effect, and as a consequence larger freshwater anomalies are needed to trigger the same behavior. The stability diagrams of the glacial climate have a distinctly different shape, the hysteresis behavior is much less pronounced. When the freshwater flux is added to the lower latitude band (20-50 °N, black curves) the modes are much closer together and the jumps are much more gradual, the response to changes in the freshwater input smoother and less obviously nonlinear. But for the latitude band corresponding to the Nordic Seas a clear jump is present near slightly negative (evaporative) freshwater fluxes. If the system is in the "cold" mode then negative freshwater anomalies in the Nordic Seas can trigger a sudden restart of the NADW formation, which leads to more energy transport into the north Atlantic and thus higher temperatures. The temperature jump is of the same magnitude as that of the switch between the modes under current climate conditions, however the hysteresis behavior is less pronounced because the involved freshwater anomaly thresholds are closer together. Therefore it is much easier for the system to switch between the modes and this is probably the reason that the North Atlantic climate is much less stable during stadial conditions than under the current climate.

They proceed by hypothesizing that there is a cycle of unknown origin within the climate system that can trigger the swifts between the modes of Atlantic circulation, and that this leads to the DO-cycle. This unobserved cycle is added to the model as a sinusoidal freshwater flux anomaly with a period of 1470 year, (which is chosen based on spectral analysis of the ice core data), the amplitude corresponds to a surface flux of roughly 300 mm/y. This means that the difference between the two extremes of the flux is 600 mm/y, which is almost as large as precipitation in the Netherlands under current climate conditions. They nonetheless state this amplitude is "very small". If the amplitude is halved no DO-events are triggered. Although it does lead to quite beautiful results one has to wonder whether the invention of this undiscovered freshwater flux anomaly cycle that is of paramount importance to these results is truly reasonable. Furthermore even though the induced freshwater fluxes are quite large the resulting temperature jumps are much smaller than those observed.

This line of research was taken one step further by Menviel et al. (2014), who used an intermediate complexity model (LOVECLIM) to calculate what freshwater fluxes are necessary to create the temperature jumps of the ice core signal. The freshwater anomalies that this leads to are of the order ±0.1 Sv, which translates into surface fluxes of about 1 m/y. For the positive freshwater fluxes this could reasonably be explained by increased melt fluxes from the ice sheet due to instabilities. However for the negative fluxes this means evaporative anomalies, so a flux of 1 m/y seems very large. Especially considering that this should occur largely prior to the DO-event, as it is supposed to trigger the restart of the AMOC. In fact the only thing that this study achieves is explaining one oscillation pattern with another, for which no real explanation is given. The temperature signal is explained by inducing a freshwater flux pattern, but this pattern remains largely unexplained. Until a reasonable explanation is given for the behavior of the freshwater flux, including an analysis of the plausibility of the magnitude of the anomalies, nothing definite is achieved and research into other processes that could influence the density driven circulation should remain open.

3.2 Autonomous oscillations

In other models the oscillations in AMOC are not dependent on periodic boundary conditions, but are internal to the system of the thermohaline circulation (THC). One of the simplest mechanisms to cause such autonomous oscillations was proposed by Broecker (1990). It works as follows; Net evaporation in the North Atlantic causes the salinities to increase to the point where NADW formation starts. This leads to an increase in AMOC activity which has a double effect, it ventilates the surface waters causing a decrease in surface salinity, and it increases melt rates of the land ice because of more northward energy transport through the ocean. The combination of these two processes leads to dropping of the surface salinities in the North Atlantic which in turn causes a slowing of the AMOC. Eventually the surface salinities drop to the point where NADW formation can't be sustained at all, causing a shutdown of the AMOC, which marks the beginning of a new cycle. Parts of this pattern however do not agree with recent observations, for example melt rates were in general higher during stadials (Kreveld, 2000).

There are also many models that do not depend on the storage and release of fresh water in land based ice that nonetheless show internal oscillations in the THC (Winton and Sarachik, 1993; Sakai and Peltier, 1995; Weaver and Hughes 1994). I will use the model by Sakai and Peltier (1995) as an example. The mechanism that is responsible for the oscillations in their model is the following: NADW formation ventilates the saline Atlantic surface waters into the deeper region, so the suppression of NADW formation leads to accumulation of salt near the surface of the North Atlantic, which increases the density and therefore eventually causes the restart of NADW formation. The restart of the AMOC leads to increased ventilation of the surface waters in the North Atlantic, which will cause salinities to drop, until eventually this starts to hinder the NADW formations again and another cycle starts. In their model a fixed time independent freshwater flux centered around 50 °N (Gaussian distribution with standard deviation of 10 °) is a control parameter on these oscillations in AMOC activity. For varying magnitudes of this freshwater flux different oscillatory modes can be produced. For freshwater fluxes of up to 1.2 m/y the overturning is relatively stable in the mode of strong overturning, although it does show small oscillations with periods on the centennial time scale. For freshwater fluxes of about 2 m/y circulation stays suppressed, but for freshwater fluxes in between these values oscillations emerge in which the AMOC switches between its "on" and "off" mode. The period of these oscillations depends on the exact magnitude of the freshwater flux anomalies, but is on millennial time scale.

A different mechanism of internal oscillation is investigated by Timmermann using the models of Gildor and Tzipermann (2001). In this model the ocean is divided into 8 boxes (4 boxes spanning the ocean from pole to pole with 2 layers each). In the results from this model the salinity doesn't play such a dominant role, the effect of temperature on the THC is more important. Figure 4 shows the development of the most relevant parameters throughout the cycle. The presence of sea ice (d) in the North Atlantic reduces the capability of the ocean to lose heat and causes a slow warming of the deeper waters (depth > 400m) through conduction (c). The warming of these waters decreases the density and leads to suppression of the THC (b). Eventually however the increase in temperature lowers the density to such an extent that the water column become unstable, and convective mixing occurs. The energy becomes available for the melting of the sea ice (d), and the removal of the sea ice in turn allows the ocean to lose even more heat (b), which leads to a sudden warming of the atmosphere (a). The release of heat causes the density of the subsurface ocean to increase again and this allows for the restart of NADW formation and the overturning circulation. This sequence of events leads to time evolution of the AMOC shown in figure 5.

How the noise level influences the periodicy of the events can be understood by looking at panel b of figure 4. The convective event that leads to the restart of the AMOC occurs when the densities of the two ocean boxes become equal. The chances of this happening soon after the last event are largely

dependent on the density perturbations in the surface ocean induced by the stochastic freshwater flux. If these perturbations are too small the instability cannot occur until the densities are brought close enough together by the warming of the subsurface ocean.

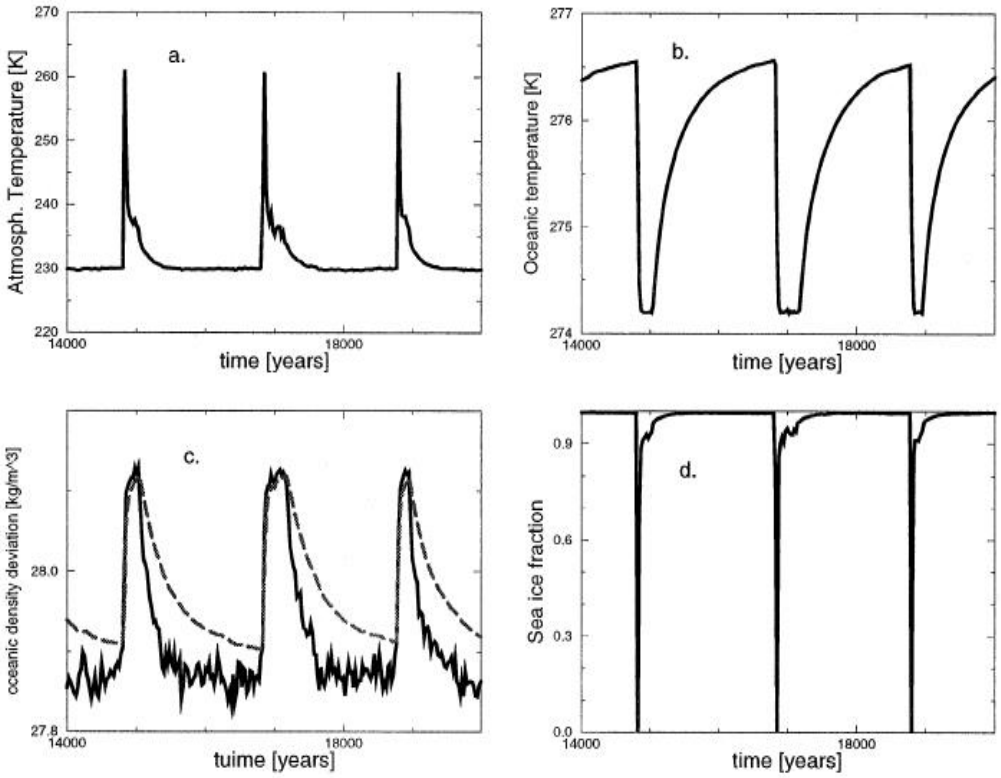

Figure 4. Januari atmospheric and oceanic variable;s (a) Atmospheric temperature, (b) oceanic subsurface temperature, (c) surface (solid) and subsurface (dashed) density, and (d) sea ice fraction. The model was initiated with a 300 year long freshwater pulse of 0.45 Sv mimicking a Heinrich event, and has a stochastic freshwater flux into the surface ocean with a standard deveiation of 0.06 Sv. From Timmermann (2003).

Although the results are very interesting the periodic instability of the water column that the whole mechanism revolves around is represented rather poorly because the ocean has only two layers. In the northern ocean circulation transports water from the surface box to the deep ocean box, this means that the circulation itself cannot warm the deep ocean box with respect to the surface box. Since if the deep ocean box is warmer than the box above it, then circulation would have a cooling effect. Therefore dividing the northern ocean in only two layers cannot capture subsurface warming caused by energy input through circulation. In order to capture this process a higher vertical resolution is necessary, as then a fresh surface layer can be established directly below the ice. In agreement with observations this surface layer is not affected directly by circulation and can thus shield the sea ice from the warming ocean below (Aagaard, 1981). This means that in order to capture this mechanism satisfactorily the ocean needs at least 3 layers.

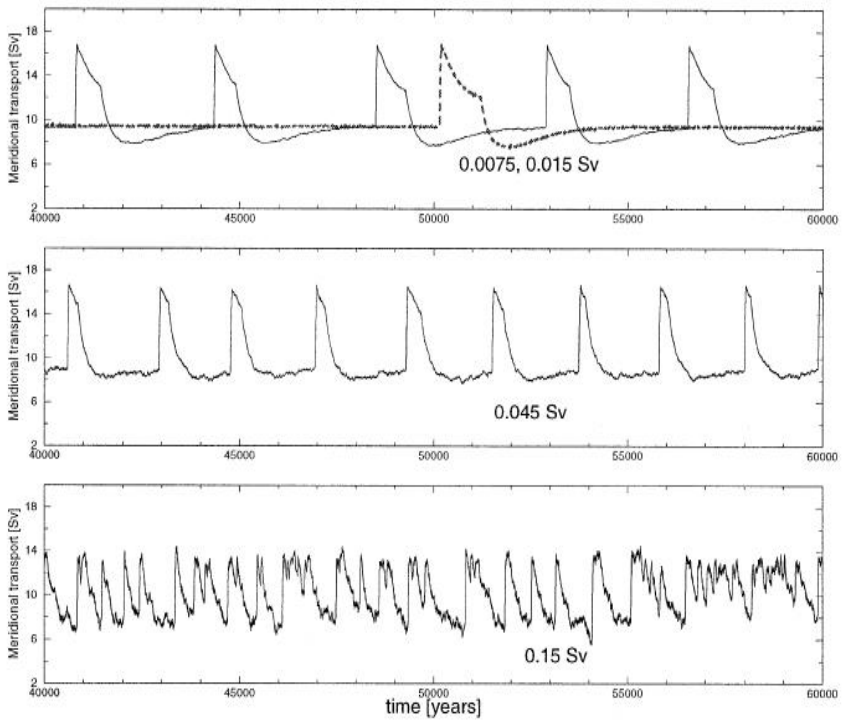

Fig 5, response of the AMOC to stochastic freshwater forcing with different amplitudes, (top) 0.075 (dashed) and 0.015 Sv; (middle) 0.045 Sv; and (bottom) 0.15 Sv. From Timmermann (2000).

A model that does capture this a little better is the model of Singh (2013). It is specifically aimed to investigate the occurrence of instabilities of a water column below sea ice caused by subsurface warming. It is based on the conceptual model by Rasmussen and Thomsen (2004) which was later expanded upon by Dokken (2013), in which increasing sea ice cover leads to stronger insulation of the ocean which in turn causes subsurface warming. This warming eventually leads to instability of the water column, causing all the energy stored in the subsurface water to be released suddenly. This causes the sea ice to melt and the atmosphere to warm.

The model consists of one water column with 4 layers representing the Nordic seas. Although the model produces an atmospheric temperature signal that has a basic structure similar to that of the observed a DO-cycles, the mechanism which causes the oscillatory behavior is not exactly that described in the conceptual model. The results of the model are shown in figure 6&7. In figure 7 it can be observed that the densities of the PC and DP layers (50-400 m and 400-1200m respectively) converge. When the density of the PC layer becomes greater than that of the DP layer (around 12500 years) the water column becomes unstable and mixing increases drastically. This leads to a sudden warming of the surface ocean, the DO-event.

Close observation of figure 6 reveals that the warming of the mid-depth ocean (DP layer) ceases long before the instability occurs. This means that the subsurface warming can't possibly be the direct cause of the instability. The reason for the continuation of the convergence of densities of the PC and DP layers, even after the temperatures of all ocean boxes has stopped changing in time, is obviously related to salinity. Ice formation and export is a net source of salt in the surface layers, causing the salinities of the top two ocean boxes (ML and PC) to increase in time. Furthermore in order for the model to conserve salt the freshwater flux related to the ice export has to be balanced. In order to achieve this a freshwater flux of equal magnitude enters the column, and under ice covered conditions this happens in the mid depth ocean (DP layer). This causes this layer to freshen in time.

Figure 6 clearly shows how it is actually this salt pump that triggers the eventual instability of the water column. In the hypothesis of Dokken (2013), upon which this model is based, the instability of the water column is triggered by subsurface warming. Even though there is this clear difference in the physical process underlying the oscillation there is no mention of this in the article. The model is presented as a case in favor of the subsurface warming hypothesis, where it actually seems to describe a new mechanism where the sea ice related salt pump leads to the instability of the water column.

Even though the changes in salinity clearly have a more important effect on the density than the changes in temperature, the parameters that determine the distribution of the salt (for example the brine injection) between the ocean layers are not taken into account in the sensitivity analysis. Another shortcoming of this model is that the energy input into column through ocean circulation is constant in time. One would expect the ocean circulation to be dependent on the state of the column, as it represents an area that strongly influences NADW formation.

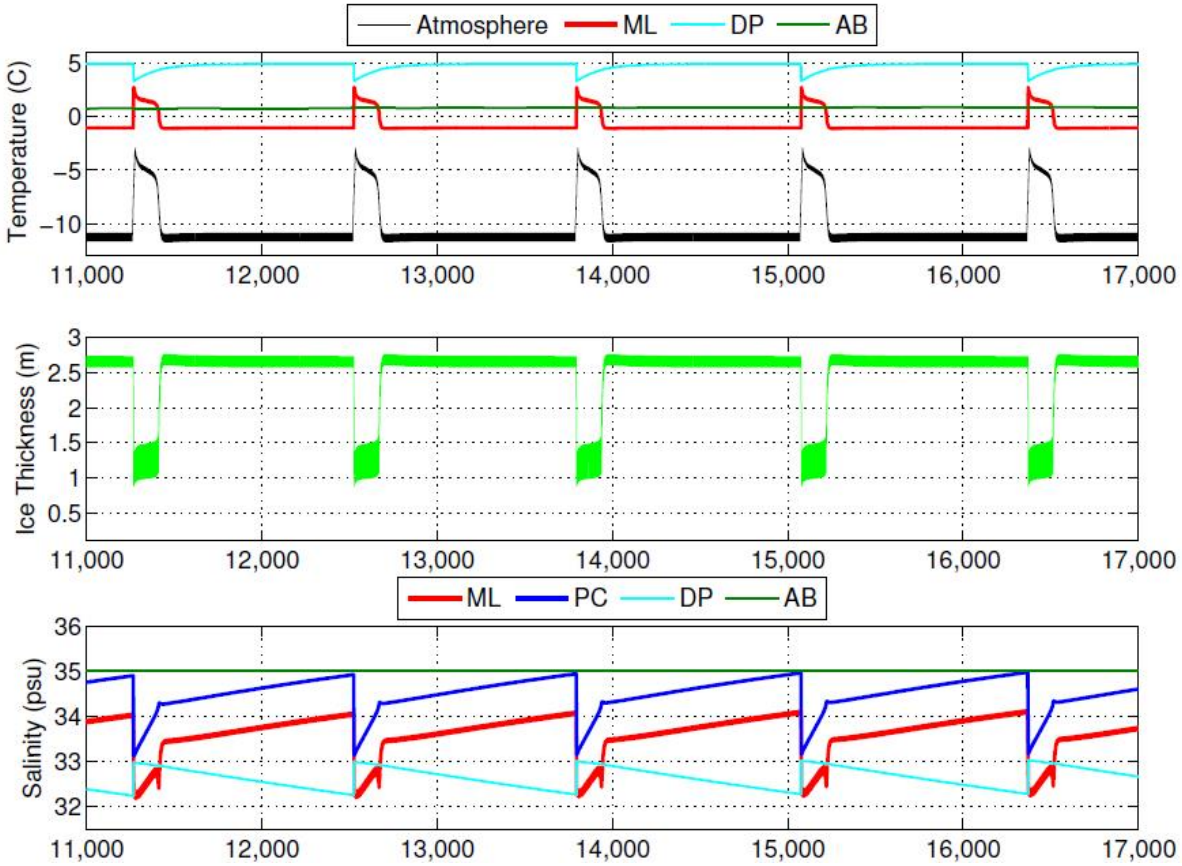

Figure 6, Temperature, ice thickness and salinity evolution in time. The ocean is divided into four boxes; mixed layer (ML) 0-50 m, pycnocline layer (PC) 50-350 m, deep ocean (DP) 400-1200 m, and abyssal layer (AB) 1200-4200 m. From Singh et al. (2013).

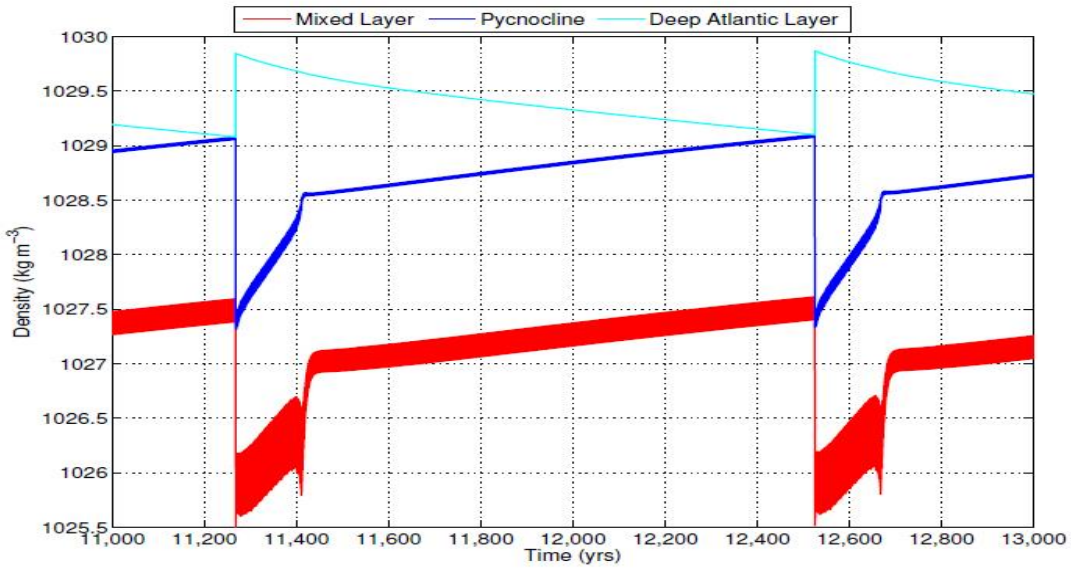

Figure 7, denstiy evolution in time for the topmost three ocean boxes; mixed layer (ML) 0-50 m, pycnocline layer (PC) 50-350 m, deep ocean (DP) 400-1200 m. From Singh et al. (2013).

3.2 Synthesis

Although there are many models capable of producing the basic structure of the DO-cycle no consensus has been reached about which best represents the actual physics. Most of the models are based upon variations in the THC and almost all of them use freshwater flux into the North Atlantic as a dominant control parameter. But as the strength of the THC can be influenced by either salinity or temperature, the question arises whether the temperature effect is really so insignificant that freshwater flux can truly be seen as the dominant control parameter. There is ample evidence of subsurface warming in the Nordic Seas during DO-stadials. This warming that is probably caused by increasing sea ice extent, could in turn be of influence on the strength of THC. One of the few model studies that does take this into account is the one by Timmermann (2003). However the model that is used (Gildor and Tziperman, 2001) only has two layers in the ocean. This means that the profiles of salt and temperature are represented very crudely and this makes a reasonable representation of the development of the stability of the water column impossible. Increasing the vertical resolution of the ocean could lead to a much better representation of the process of subsurface warming below the ice.

The strength of the AMOC is of influence of the amount of energy transported into the North Atlantic, and this in turn is of influence on the sea ice extent. On the other hand the sea ice extent itself could influence the AMOC through density changes in the water below the ice. The density can decrease as a consequence of the warming that occurs due to increased insulation. To gain further insight into this interaction would take a model that captures both processes in a satisfactory fashion. Of course it would be the best if this interaction could be mimicked with full AOGCM, but these are in general too costly for long integrations. Studying these processes with a highly simplified model might not lead to solid conclusions about the physics underlying the DO-cycle, it could nonetheless lead to interesting insights into the possible role and functioning of this interaction.

4 Model description

4.1 Introduction

In order to study the effect of subsurface warming at high latitudes as a consequence of increasing sea ice extent on the strength of THC, a new model needs to be created that includes both these mechanisms in a satisfactory fashion. The ocean box representing the North Atlantic should have a vertical resolution that can capture the most important aspects of the profiles of salinity and temperature. It is not necessary for the rest of the ocean to have a similar vertical resolution, as the only point of interest is to gain an indication of how the changes in the column representing the North Atlantic influence the strength of the THC. To achieve this the column is embedded in a "Stommel model" (Stommel, 1961). As observations show that the DO-cycle is linked to the Heinrich events an ice sheet is added to the model, which is connected to the column through an ice shelf.

In the creation of this model the processes that are most relevant to the phenomena that are to be studied have been isolated. A benefit of this approach with respect to developing a model that tries to encapsulate all the physics in the most elaborate way possible, is that a simple model can give a clearer view on the mechanisms involved. Separating the dominant processes and studying these in isolation is a way of developing understanding with respect to the functioning of the separate mechanisms and their interaction. Whereas in studies with models that try to capture as much physical processes as possible the understanding of the large scale patterns can sometimes get lost in too much detail. However once the patterns are discovered in basic models, they can be a guideline for further investigation with more elaborate models. It can then be investigated if the pattern holds as more and more interacting processes are added. It is in this orientating way that this model should be viewed. Many readers might have objections with the assumptions that are made, or the simplicity of the parameterizations. Please remember that this is not intended as a depiction of reality, it is intended as a tool to help gain understanding of some of the mechanisms that shape it.

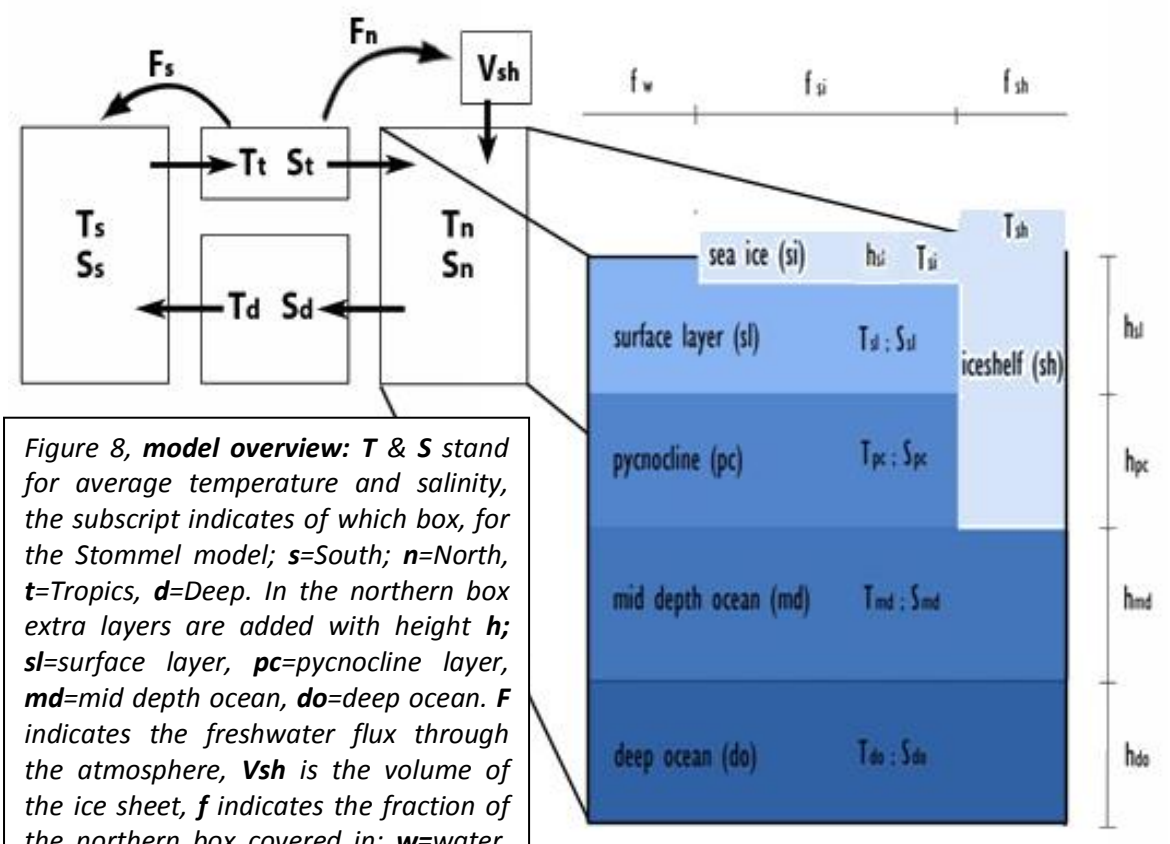

Figure 8, ***model overview: T*** *&* ***S*** *stand for average temperature and salinity, the subscript indicates of which box, for the Stommel model;* ***s****=South;* ***n****=North,* ***t****=Tropics,* ***d****=Deep. In the northern box extra layers are added with height* ***h;*** ***sl****=surface layer,* ***pc****=pycnocline layer,* ***md****=mid depth ocean,* ***do****=deep ocean.* ***F*** *indicates the freshwater flux through the atmosphere,* ***Vsh*** *is the volume of the ice sheet,* ***f*** *indicates the fraction of the northern box covered in;* ***w****=water,* ***si****=sea ice,* ***sh****=ice shelf.*

4.2 Overview

The model consists of a 4 box Stommel model with a 4 layer column embedded within the northern box, as shown in figure 8. In the figure all the model variables are shown: each ocean box has average temperature and salinity, denoted by T and S respectively, the subscript denotes which box is concerned (for the Stommel model; **s**=South, **n**=North, **t**=Tropics, **d**=Deep, and for the column model; **sl**=Surface layer, **pc**=Pycnocline layer, **md**=Mid-depth ocean layer, and **do**=Deep ocean layer). The surface of the column can be open water, covered by sea ice or covered by an ice shelf. The fraction of each surface type is referred to as 'f_{ow}', 'f_{si}' and 'f_{sh}' respectively. The sea ice is characterized by a thickness and a surface temperature; h_{si} and T_{si} respectively. The ice sheet has a variable volume, V_{sh}.

In the Stommel model the strength of the circulation is calculated from the density difference between the southern box and the northern box. The fluxes between the boxes depend on the strength of the circulation and the temperatures/salinities of the boxes involved. The atmospheric freshwater fluxes from the tropics to the polar boxes are added as negative salt fluxes, which are fixed. The southern and tropical box adapt to an equilibrium temperature on a given time scale.

Within the column model, for convenience all the fluxes are normalized with respect to the column surface, (so the fluxes leaving the column towards the other boxes must be multiplied with the total surface of the column). Between the layers there are energy fluxes and salt fluxes, indicated with symbols Q and W respectively. Where a flux at the interface between two layers is concerned, the subscript will consist of the abbreviations of both layers. Fluxes of energy and salt at the ice surface will be denoted by a combination of the relevant ocean layer and subscript '**si**' or '**sh**' for the sea ice and ice shelf respectively. The topmost ocean box is assumed to be in radiative equilibrium with the atmosphere and turbulent fluxes are related to the surface temperature. If the temperature of the surface layer drops below freezing point then sea ice forms. The volume of ice that is formed is calculated by assuming that all the energy needed to raise the temperature of the surface layer back to freezing point comes from the latent heat released during ice formation. When ice is initially formed it has a fixed thickness, so the ice extent can be related to the volume. Only when the column is fully covered with ice does a further increase in ice volume lead to an increase in ice thickness. The model can also be run with inclusion of an ice sheet/shelf. The shelf thickness equals that of the topmost two ocean boxes, so it stands into direct contact with the mid depth ocean box. The outflow of the sheet into the shelf is dependent on the sheet height and the melt rate of the shelf. An overview of all the parameters used in the model is given in appendix 1.

4.3 Assumptions

- Freshwater from ice melt flows into the surface layer, brine formed during ice formation is distributed in unequal amounts over the top three layers.
- The depth at which the inflow from the Atlantic into the northern box takes place is influenced by the sea ice cover. When the column is ice free this flux enters the column closer to the surface, but when the column is covered with sea ice it enters below the halocline (Aagard et al., 1981)
- The amount of sea ice cover is of influence on the strength of the mixing between the top three ocean boxes.
-Each year a fixed percentage of the total sea ice is transported out of the northern box by wind and currents, (it is added to the "tropical box" as a freshwater flux).
-The heat flux into the ice shelf at the frontal boundary is neglected because horizontal length scales are much greater than those in the vertical.

4.4 Equations

4.4.1 Stommel model

The Stommel model is constructed following Zickfeld (2004). The strength of the thermohaline circulation is related to the difference in density between the northern and the southern box, with:

$$F_{th} = k\frac{(\rho_n - \rho_s)}{\rho_0} \quad (1)$$

In which F_{th} is the strength of the thermohaline circulation, k ($25.4 \cdot 10^{17} m^3/y$) is a hydraulic coefficient relating the density difference to a water volume transport, and ρ_0 is a reference density. All parameters are listed in appendix 1. The density of the northern box ($\boldsymbol{\rho}_n$) is simply the average density of the water column. The temperature change due to circulation can be expressed as a volume flux multiplied by the temperature difference of the water that is transported into the box and that being transported out of it, divided by the volume of the box. Next to temperature changes induced by circulation, the temperatures of the Southern and Tropical box change due to energy exchanges at the surface. Instead of formulating the energy balance, they simply adapt to an equilibrium temperature on a given time scale. This leads to the following equations:

$$\frac{dT_s}{dt} = \frac{F_{th}}{V_s}(T_d - T_s) + \frac{F_{wd}}{V_t}(T_t - T_s) + \lambda_s\left(T_s^{eq} - T_s\right) \quad (2)$$

$$\frac{dT_t}{dt} = \frac{F_{th}+F_{wd}}{V_t}(T_s - T_t) + \frac{F_{wd}}{V_t}(T_n - T_t) + \lambda_t\left(T_t^{eq} - T_t\right) \quad (3)$$

$$\frac{dT_d}{dt} = \frac{F_{th}}{V_d}(T_n - T_d) \quad (4)$$

In which F_{th} is the volume flux due to thermohaline circulation, and F_{wd} is the volume flux due to wind driven circulation. The V's are the volume of the ocean boxes, the T^{eq}'s are equilibrium temperatures that the ocean box adapts to, and the λ's are timescales of this adaption, given by:

$$\lambda_s = \frac{\boldsymbol{\Gamma}}{c_p \rho_0 z_s} \quad \text{and} \quad \lambda_t = \frac{\boldsymbol{\Gamma}}{c_p \rho_0 z_t} \quad (5\&6)$$

In which Γ is a thermal coupling constant ($7{,}3 \cdot 10^8$ J/y/m^2/C), c_p is the specific heat of water, ρ_0 is a reference density and z is the thickness of the box (the value of all parameters can be found in appendix 1). The salinity changes can be expressed in a similar fashion:

$$\frac{dS_s}{dt} = \frac{F_{th}}{V_s}(S_d - S_s) + \frac{F_{wd}}{V_s}(S_t - S_s) - \frac{F_s S_0}{V_s} \quad (7)$$

$$\frac{dS_t}{dt} = \frac{F_{th}+F_{wd}}{V_t}(S_s - S_t) + \frac{F_{wd}}{V_t}(S_n - S_t) + \frac{(F_s+F_n-F_{ice})S_0}{V_t} \quad (8)$$

$$\frac{dS_d}{dt} = \frac{F_{th}}{V_d}(S_n - S_d) \quad (9)$$

In which S_0 is a reference salinity, and F_s and F_n are prescribed south- and northward atmospheric freshwater fluxes, and F_{ice} is the freshwater flux from the northern box to the tropical box related to the transport of ice.

4.4.2 Radiation

The daily average insolation is calculated as a function of the time before present and latitude, this is done using the equations of Berger (1991). Milankovitch variations in eccentricity, obliquity and precession are taken into account. The exact equations can be found in the original article and will not be treated here. As the surface of the column can be either open water, sea ice or covered by an ice shelf, the short wave radiation is split into these three separate cases. So the total net shortwave radiation is given by:

$$S_{net} = \big(f_{ow}(1-\alpha_w) + (f_{si}(1-\alpha_{si}) + (f_{sh}(1-\alpha_{sh})\big)S_{in}\,(1-C_{cloud}) \tag{10}$$

In which α_w and α_{si} and α_{sh} are the albedo's of water, sea ice and the shelf respectively. C_{cloud} is a cloudiness coefficient, it has value between 0 and 1, (when it has value 0 no radiation is reflected by clouds at all, and if it has value 1 all the shortwave radiation is reflected by clouds.) By assuming the surface to be in radiative equilibrium with the atmosphere above it, and using a linearization of the Stefan Boltzman law around 0 °C, the longwave radiation equation can be written as:

$$L_{net} = -\frac{A+BT}{n} + \frac{D}{2} \tag{11}$$

in which $A \approx \sigma T_0^4 \approx 320 W/m^2$ and $B \approx 4\sigma T_0^3 \approx 4{,}6 W/m^2/K$, n is a measure for the optical thickness of the atmosphere (the average photon crosses 1/n of the atmosphere before it collides) and is dependent on the season because of the varying water content. As the water content of the atmosphere has a different yearly cycle over water than over ice, in the model two different sinuses are used, both with a period of one year. Following Singh (2013) over water we will use the values 2,7 for the mean and 0,4 for the amplitude. Over ice the slightly different values of mean=2,65, and amplitude=0,3 are used. The symbol D is a measure for the convergence of the horizontal energy flux through the atmosphere. If there is a net positive energy flux into the atmosphere column then D has a positive value and this has a warming effect. This equation is applied to each of the surface types, as each has a different surface temperature. As D is a measure for the temperature of the atmosphere stochastic perturbations are added to this value to create random year to year variation. Because day to day variations are of no interest to the model results, for stability reasons the perturbations are only changed once every year:

$$D = D_{mean} + \sigma(D_{amp}) \tag{12}$$

4.4.3 Ocean thermodynamics

As the surface of the surface layer can be either open water or sea ice, the fluxes through the surface are multiplied by the fractions of that surface type. The heat input from the pycnocline layer is also multiplied by the dimensionless area of the interface, which is the fraction not covered by shelf:

$$m_{sl}c_p\frac{dT_{sl}}{dt} = f_{ow}(S_{in}(1-\alpha_w) + L_{net} - Q_{turb}) - f_{si}Q_{sl-si} + (1-f_{sh})Q_{pc-sl} + Q_{A\,sl} \tag{13}$$

in which; m_{sl} is the mass of the surface layer, (given by $m_{sl} = (1 - f_{sh})h_{sl}\rho_{sl}$), and c_p is the heat capacity of water, S_{in} is the incoming shortwave radiation, α_w is the albedo of water, L_{net} is the net longwave radiation, Q_{turb} is the sum of the turbulent fluxes, which are calculated using a bulk approximation (Peixoto and Oort 1992) (given by *eq.14)*, and $Q_{A\,sl}$ is energy advected into the surface layer by the THC.

$$Q_{turb} = C_{turb}(T_{sl} - T_0) \qquad (14)$$

in which C_{turb} is the turbulent exchange coefficient, and T_{min} is the minimum temperature that the surface layer can have (-1.8°C).

The second term on the R.H.S. in *eq.13* is the product of the fraction sea ice and the flux from the surface layer into the ice. This flux is again calculated with a bulk equation, using a fixed temperature for the ice water interface:

$$Q_{sl-si} = C_{si}(T_{sl} - T_0) \qquad (15)$$

In which C_{si} is a coefficient linking the flux to the gradient, and T_0 is the temperature at the ocean sea ice interface. All the energy fluxes between the ocean boxes are calculated from gradient between the layers, they are expressed as:

$$Q_{i-j} = \frac{2K^T c_p(T_i\rho_i - T_j\rho_j)}{h_i + h_j} \qquad (16)$$

The K coefficient can be found in appendix 1. The mixing between the top three layers depends on the ice cover, because ice cover shields the ocean from winds, and therefore decreases the amount of mixing. Between the values for an ice free and a totally covered column the coefficient is determined using a linear interpolation. The last term in *eq.13* is the energy transported into this layer from the Atlantic. The total influx into the column comes directly from the Stommel, but because the column is normalized with

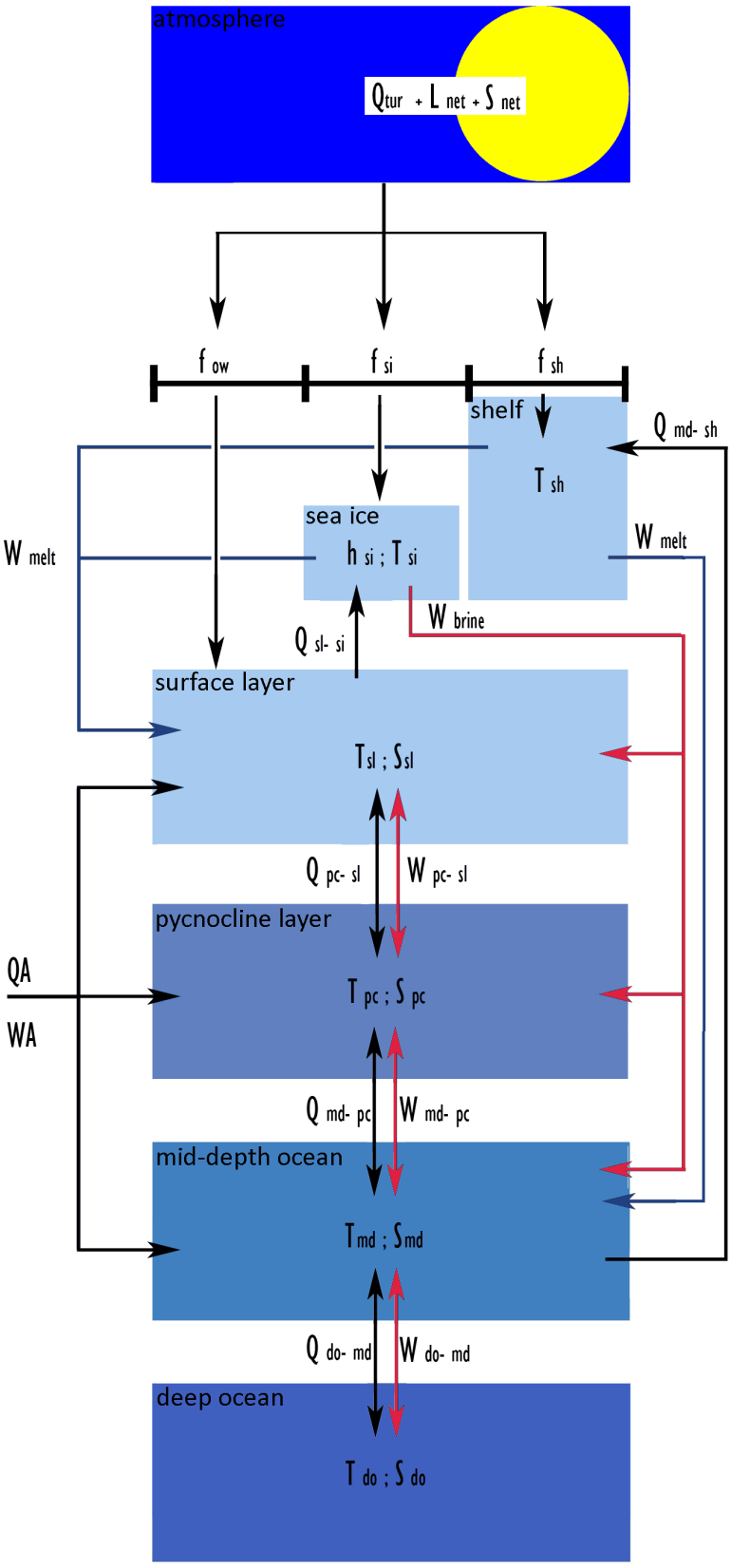

Figure 9, The overview of the fluxes between the various boxes. Q's are energy fluxes, and W's denote salt fluxes. For each of the surface types a separate energy balance is made.

respect to its surface it is written in a slightly different form (it is expressed in W/m^2):

$$Q_A = \frac{C_{TH}\,(T_t - T_n)\,\rho_0\,c_w}{A_n} \tag{17}$$

In which A_n is the area of the northern box. If there is no ice cover there is inflow close to the surface, whereas when the column is fully ice covered the water enters the column below the halocline (below the fresh surface layer, the flux that would normally enter the surface layer is added at greater depth). This is consistent with the observations of Aagaard (1991) who showed that water transported into the Arctic from the Atlantic will follow isopycnals and subducts beneath the halocline. Between the two extremes the distribution is calculated using a linear interpolation. This leads to following fluxes for each layer;

$$Q_{A\,sl} = f_w J_{sl} Q_A \tag{18}$$

$$Q_{A\,pc} = J_{pc} Q_A \tag{19}$$

$$Q_{A\,md} = (J_{md} + (1 - f_w) J_{sl}) Q_A \tag{20}$$

In which Q_A is the total heatflux from the Atlantic, and the *J's* are factors determining the distribution of energy between top three boxes. Analogously to *eq.13* the following energy balance can be derived for the pycnocline layer;

$$m_{pc} c_p \frac{dT_{pc}}{dt} = (1 - f_{sh})(-Q_{pc-sl} + Q_{md-pc}) + Q_{A\,pc} \tag{21}$$

For the mid depth ocean there is the extra term for the flux into the bottom of the ice shelf (see figure 8). This leads to:

$$m_{md} c_p \frac{dT_{md}}{dt} = -(1 - f_{sh}) Q_{md-pc} - f_{sh} Q_{md-sh} + Q_{do-md} + Q_{A\,md} \tag{22}$$

In which $\mathrm{Q_{md-sh}}$ is the heat flux into the ice shelf, given by:

$$Q_{md-sh} = C_{sh}(T_{md} - T_0) \tag{23}$$

In which C_{sh} is a coefficient linking the flux to the gradient, and T_0 is the temperature at the ocean ice shelf interface. The energy balance for the deep ocean is very simple as it only interacts with the mid depth ocean layer:

$$m_{do} c_p \frac{dT_{do}}{dt} = -Q_{do-md} \tag{24}$$

4.4.4 Sea ice

To initialize the sea ice growth a scheme is used in which sea ice forms automatically if the temperature of the surface layer drops below the freezing point (-1,8 C). When the surface layer temperature becomes lower than freezing point the temperature of the surface layer is set back to freezing point, the energy used for this is assumed to come from the latent heat of fusion. This means that in this case the ice volume can be expressed in the following equation:

If $T_{sl} < T_0$, then $dV_{si} = \frac{(T_0 - T_{sl}) h_{sl} \rho_{sl} c_p}{L_f \rho_i}$ (25)

In which L_f is the latent heat for fusion. This creates ice with a fixed thickness, so the volume can directly be related to the ice extent (fraction). Only when the whole surface of the column is covered with ice does the ice thickness increase. When the ice reaches a critical fraction the ice formation is calculated in a different manner, the energy balance at the bottom of the sea ice is considered. The ice grow (or melt) is determined by flux divergence (convergence) at the ocean-sea ice interface. If the ocean provides more energy than is transported upwards through the ice, then this energy is used for melting. On the other hand, if the conductive heat flux through the ice is greater than that which the ocean provides then this leads to ice formation. The temperature at the ocean-sea ice interface is kept constant, so both fluxes can be calculated from the gradients. The first is determined with a bulk method from the temperature difference between the ice bottom and the underlying ocean, and the second is determined by the temperature gradient through the sea ice:

$$Q_{sl-si} = C_{si}(T_{sl} - T_0) \quad \text{and} \quad Q_{con} = \frac{K_{ice}(T_0 - T_{si})}{h_{si}} \tag{26}$$

In which C_{si} is bulk coefficient relating the flux to the gradient at the ocean-sea ice interface, T_0 is the freezing point of sea water (-1.8°C), K_{ice} is the conductivity of sea ice, and T_{si} is the temperature of the ice surface. This leads to the following equation for the sea ice volume change:

$$\frac{dV_{si\,bottom}}{dt} = f_{si}(Q_{con} - Q_{sl-si})/(\rho_{ice}L_f) \tag{27}$$

The temperature at the sea ice surface is calculated from the energy balance at the surface. The net energy balance is used to calculate the new surface temperature (assuming a linear profile through the sea ice it can be related to the 'area' of the triangle, because this is actually a volume times a temperature change). This leads to the following equation for the temperature change at the surface:

$$\frac{dT_{si}}{dt} = 2(Q_{con} + S_{net} + L_{net})/(h_{si}\rho_{si}c_{p\,ice}) \tag{28}$$

Due to the parameterization of the longwave radiation the turbulent fluxes are neglected. If the surface temperature becomes greater than freezing, it is automatically set back to freezing point. The energy that disappears by doing this is used for melting the ice, this leads to the following relation:

If $T_{si} > 0$, then $\quad dV_{si\,surf} = -f_{si}\frac{1}{2}h_{si}T_{si}\frac{c_{p\,ice}}{L_f}$ (29)

Each time step a certain amount of ice is transported out of the column by winds and currents, on a yearly basis this is a fixed percentage of the average total amount of ice, this is given by:

$$\int_{1\,year} \frac{dV_{si\,export}}{dt}\, dt = -C_x\overline{V_{sl}} \tag{30}$$

In which C_x is the percentage of sea exported on a yearly basis, and $\overline{V_{sl}}$ is the yearly average sea ice volume. Adding all these terms together lead to the full equation for the development of the sea ice volume:

$$\frac{dV_{si}}{dt} = \frac{dV_{si\,bottom}}{dt} + \frac{dV_{si\,surf}}{dt} + \frac{dV_{si\,export}}{dt} \tag{31}$$

4.4.5 Salt

For each layer the salt budget is calculated in grams of salt, the salinity can be calculated from this by dividing by the total mass of the layer. The salt fluxes between the layers are calculated from the gradients, the coefficients can be found in appendix 1.

$$W_{i-j} = \frac{2K^S(S_i\rho_i - S_j\rho_j)}{h_i + h_j} \tag{32}$$

The salt flux due to brine release during ice formation can be expressed as follows:

$$W_{brine} = \rho_i \frac{S_0}{\left(1-\frac{S_0}{1000}\right)}\left(\frac{dV_{ice}^{growth}}{dt}\right) \tag{33}$$

In which S_0 is a reference salinity used to calculate the salt fluxes due to formation and melt of sea ice. It follows that the freshwater flux caused by the melting of ice should lead to a negative salt flux, that is expressed in a similar way. The fresh water released during the melting of the sea ice and the top the shelf all enters the surface layer. The brine released during the sea ice creation and the melt from the bottom of the shelf is distributed over the top three ocean boxes (see figure 9). This leads to the following equations for each layer for the development of the amount of salt over time:

$$m_{sl}\frac{d\boldsymbol{S}_{sl}}{dt} = (1-f_{sh})W_{pc-sl} + \rho_i \frac{S_0}{\left(1-\frac{S_0}{1000}\right)}\left(\frac{dV_{si}^{melt}}{dt} + \frac{dV_{sh\,top}^{melt}}{dt}\right) + B_{sl}W_{brine} + W_{A\,sl} - W_{sheet} \tag{34}$$

The first term is the flux over the interface between the surface layer and the pycnocline layer. The second term is the freshwater input due to ice melt. The third term represents the brine that mixes in the surface layer while sinking, the *B* coefficients represent the fractions of the total amount of brine that is added to each individual layer (The B coefficients of the top three layer add up to 1). The fourth term, $W_{A\,sl}$is the salt influx from the Atlantic. The last term is the negative salt flux associated with the melt of the ice sheet. Analogously the salt budgets for the other layers are expressed as:

$$m_{pc}\frac{d\boldsymbol{S}_{pc}}{dt} = -(1-f_{sh})W_{pc-sl} + W_{md-pc} + B_{pc}W_{brine} + W_{A\,pc} \tag{35}$$

$$m_{md}\frac{d\boldsymbol{S}_{md}}{dt} = -W_{md-pc} + W_{do-md} + \rho_i \frac{S_0}{\left(1-\frac{S_0}{1000}\right)}\left(\frac{dV_{sh\,bot}^{melt}}{dt}\right) + B_{md}W_{brine} + W_{A\,md} \tag{36}$$

$$m_{do}\frac{d\boldsymbol{S}_{do}}{dt} = -W_{do-md} \tag{37}$$

The salt transported into the column follows from the Stommel model. Because it has to be normalized with respect to the area of the column it can be expressed as:

$$W_A = \frac{C_{TH}\,(S_t - S_n)\,\rho_0}{A_n} \tag{38}$$

The salt is distributed over the top three layers similar to the energy, see *eq. 18-20*.

4.4.6 Density

The density of layers is calculated using the full Gibbs seawater equations (Feistel, 2003), which for obvious reasons are not included here. When the density of an underlying layer becomes smaller than that of layer above it instability occurs and both layers are instantaneously totally mixed.

4.4.7 Land ice

To add the Heinrich events to the model an ice sheet is implemented that interacts with the ocean through outlet glaciers/an ice shelf. (The part of the ice sheet that in contact with the ocean will from now on be referred to as the ice shelf). The volume of the shelf is related linearly to the volume of the sheet through the expressions:

$$R\,V_{sheet} = V_{shelf}^{eq} \qquad \text{which leads to;} \qquad f_{sh}^{eq} = \frac{R\,A_{sheet}\,h_{sheet}}{A_n\;h_{shelf}} \tag{39}$$

In which f_{sh}^{eq} is the equilibrium shelf extent, where the combination of blockage by the shelf mass and friction would exactly balance the pressure of the sheet height. It is the extent that the shelf would reach in the absence of melt. The outflow can now be related to the deficit between the actual extent and the equilibrium extent through:

$$\frac{df_{sh}^{flow}}{dt} = \frac{1}{\tau_f}\left(f_{sh}^{eq} - f_{sh}\right) \tag{40}$$

In which τ_f is a time scale that relates the shelf deficit to the flow speed (It is the time it would take the ice flow to close the deficit if the ice flowed continuously with that speed). It is assumed that an increase in the flow speed in the ice streams reduces the basal friction. But when the friction is reduced the ratio R (in eq. 39) is influenced, as more blocking shelf mass will be needed for the system to be in balance under the same ice sheet height. This means that R becomes a function of the flow speed. It will be assumed that under a certain flow speed threshold changes in the flow speed do not influence the friction, however when the flow speed passes this threshold the friction will slowly to decrease. It is furthermore assumed that after a certain point a further increase in flow speed will no longer influence the friction. This leads to the following expressions:

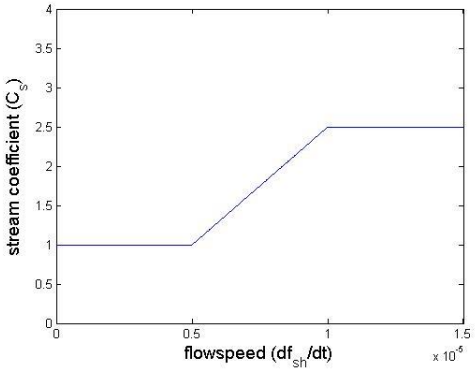

Figure 10, dependence of the stream coefficient on the flow speed

$$R = R_{min}C_s \tag{41}$$

In which R_{min} is the minimal value the ratio has, and C_s is the stream coefficient. The dependence of the stream coefficient on the flow speed is plotted in figure 10. To complete the set of equations we only need equations for the mass balance of the sheet and the shelf. For the sheet it can be expressed as:

$$\frac{dV_{sheet}}{dt} = A_n(P - M) - \frac{dV_{flow}}{dt}, \text{ which leads to: } \quad \frac{dh_{sheet}}{dt} = \frac{A_n}{A_{sheet}}\left(P - M - \frac{df_{sh}^{flow}}{dt}h_{shelf}\right) \tag{42}$$

In which *P* is the precipitation and *M* is the melt (which in order to make the model salt conserving are related back to the moisture flux through the atmosphere in the Stommel model (F_n in eq. 8), a fixed percentage (P_p) is added to the sheet, the rest is added to the surface layer). In the energy balance of the shelf there is mass gain through inflow from the sheet, and mass loss through melt. Precipitation on the shelf is neglected. There is an additional export term that is related to ice bergs being transported out of the column. This leads to the following equation:

$$\frac{df_{sh}}{dt} = \frac{df_{sh\,flow}}{dt} - \frac{1}{h_{sh}}\left(\frac{dV_{shelf}^{melt}}{dt} + \frac{dV_{shelf}^{export}}{dt}\right) \tag{43}$$

In which;

$$\frac{dV_{sh\,melt}}{dt} = \frac{dV_{sh\,melt}^{top}}{dt} + \frac{dV_{sh\,melt}^{bottom}}{dt} = \frac{-f_{sh}}{L_f \rho_i}\Big(\big((1-\alpha_{sh})S_{in} + L_{net}\big) + C_{sh}(T_{md} - T_0)\Big) \tag{44}$$

$$\frac{dV_{shelf}^{export}}{dt} = C_s^{sh}\frac{dV_{shelf}^{melt}}{dt} \tag{45}$$

In *eq. 44* the energy that is used for melting at the top of the shelf is expressed as function of the energy balance at the surface. At the bottom of the shelf the energy flux is related to the temperature difference between the ocean and a fixed temperature of the bottom of the shelf. The volume of ice transported out of the column is assumed to be a linear function of the melt volume as expressed in *eq.45*.

4.4.8 Numerical methods

The Euler forward method has been used to discretize the time derivates found in the model equations. A time step of 1 day is used.

5 Results

5.1 Dansgaard-Oeschger events

The model is run with the default values listed in appendix 1. To spin up the model it has been run for 10000 years with reasonable initial conditions, the average values over the last 100 years were used as the new initial conditions. The most important forcing of the model is the shortwave radiation, it is calculated with the equations of Berger (1991). Another important forcing term is D, the average convergence of the atmospheric heat flux over the column. As this parameter is a measure for the temperature of the atmosphere, a stochastic perturbation has been added to add some year to year variation (Every year a random value with a standard deviation of 10 W/m^2 is added to a mean value of 110 W/m^2).

Figure 11 shows the yearly average of the sea ice thickness (panel A) and the salinity (B), temperature (C) and density (D) of the different layers of the column *(sl=surface layer, pc=pycnocline layer, md=mid depth ocean layer, do=deep ocean layer)*. The time scale on the x axis is in model years. In figure 11 a representative selection of 2500 years of the entire model run (18000 years) is shown.

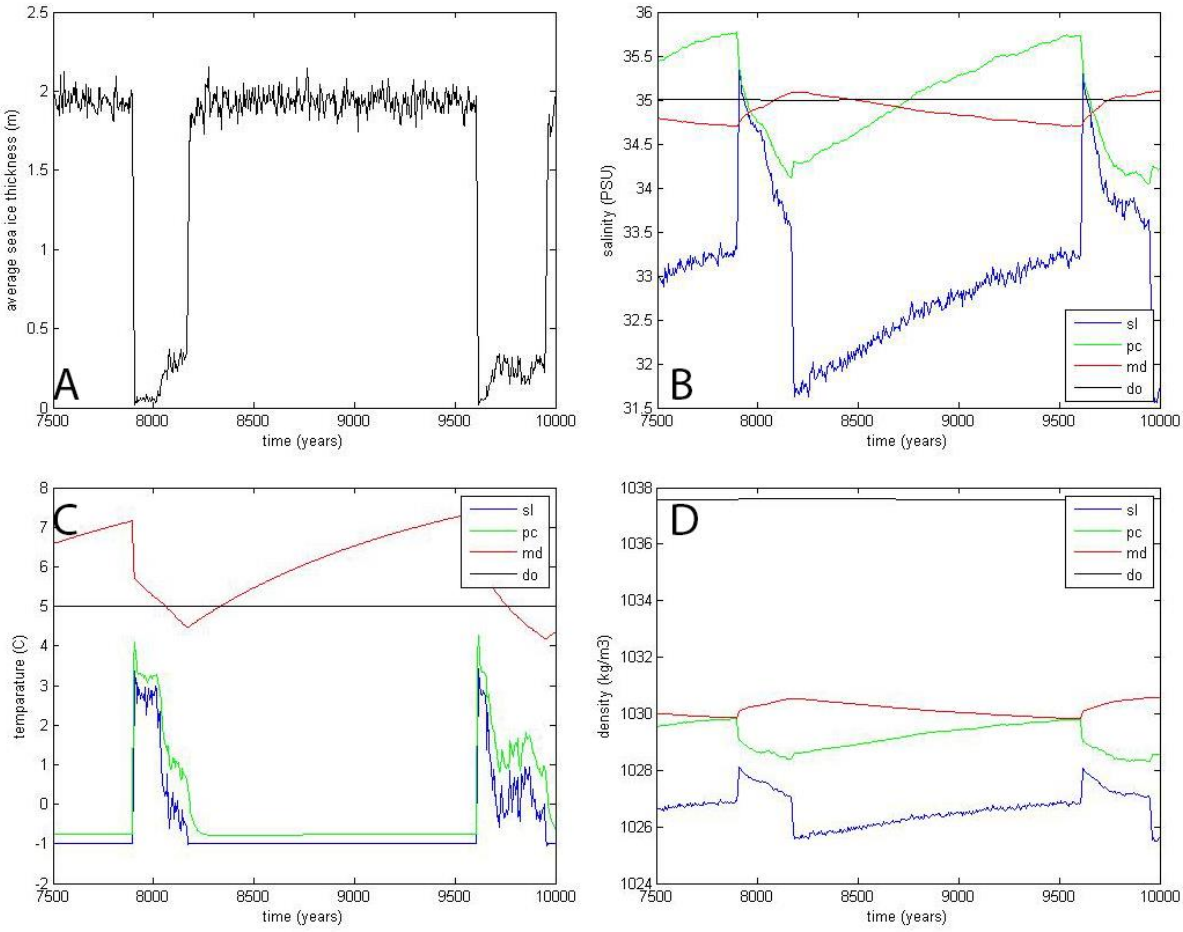

Figure 11, yearly averages of ice thickness(A), salinity (B), temperature (C) and density (D) of the various layers of the column model (sl=surface layer; pc=pycnocline layer; md=middepth ocean layer and do=deep ocean).

In panel A it can be seen that around 8000 the sea ice thickness is less than 0,5 m, this means that the column is not fully covered year round (as the minimal ice thickness in the model is 0,5 m). After 8200 years however the sea ice remains throughout the year. The state with seasonal ice cover is an unstable state, as the ice albedo feedback pushes the system towards more ice cover. The fully covered state is stable because when the ocean is fully covered insufficient solar energy can be absorbed during the summer to melt enough of the ice to break the ice cover. The only way the system can get out of the fully covered state is through a DO event, these events occur when the water column becomes unstable. It can be observed in panel D that the lines of the pc- and md-layer touch, starting convective mixing (for example at 7900 years).

The annual cycle of the sea ice thickness has an average amplitude of about 1 meter (not shown). This ice growth and melt act as a salt pump, the fresh melt water stays in the surface layer, but part of the brine produced during the ice formation sinks to the deeper layers. Panel B shows the effect of this on the salinities of the various layers. During interstadials (period 7900-8200 and 9600-10000 years) there is open water during the summer, this allows wind driven mixing to take place and thus prevents the establishing of a true fresh surface layer. However from the moment the sea ice becomes perennial mixing is reduced all year round, and a fresh surface layer forms directly below the sea ice. As part of the sea ice is transported out of the column the annual sea ice growth and melt do not exactly balance. More ice forms than is melted, and this leads to a net salt flux into the two topmost layers. It can be observed that during the stadials these layers *(surface layer and pycnocline layer)* gradually become more salty, although of course the surface remains relatively fresh compared to the other layers. From the moment sea ice becomes perennial the annual amount of sea ice growth and melt are reduced, because the net input of solar energy into the system is lower. This causes a lowering of the salt fluxes related to brine, and it can be observed in panel B that as a consequence of this the mid-depth ocean layer freshens due to advection and shelf melt.

Panel C shows the temperatures of the layers, it can be observed that during the stadials when the ice cover is perennial, the top two layers are close to the temperature of the bottom of the ice. In contrast to salinity the biggest temperature gradient is between the pycnocline layer and the mid depth ocean layer. This is in agreement with observations, as measured profiles of temperature and salinity below the sea ice often show a thermocline that is at greater depth than the halocline (for example; Aagard, 1981). The reduction in wind driven mixing means that the mid- depth ocean is hindered in its capacity to lose heat. As there is still an energy influx from the Atlantic this has a net warming effect on the mid depth ocean. The total amount of subsurface warming during a stadial of about 3,5°C corresponds well to observations. It is well within the range suggested by Rasmussen & Thomson (2004), but slightly higher than the moderated range suggested by Dokken (2013). During the DO-event the convective mixing leads to a sudden heat transport towards the surface. The mid-depth ocean cools, and the surface and pycnocline layers become warmer. During the interstadial the mid depth ocean layer cools further, as the layer can release more heat to the surface because the wind mixing is stronger due to the lack of a sea ice cover. The increase in the amount of mixing causes the mid-depth ocean temperature to approach to the pycnocline layer temperature.

The densities of the layers are influenced by both the salinity and the temperature. The time evolution of density is shown in panel D. It becomes clear that the gradually increasing salinity of the pycnocline layer, in combination with the increase in temperature of the mid depth ocean, leads to the convergence of the densities of these layers. This results in an instability of the column at 7900 and 9600 years. These are the DO-events. Density driven convection leads to a sudden increase in the vertical mixing and this means that the energy stored in the mid depth ocean is suddenly released. It leads to the melting of the sea ice (panel A), which in turn leads to a further increase in mixing.

The system has now returned to the interstadial mode, but this mode is not fully stable. The energy released from the ocean allows the system to remain in this mode for a while, but after the surplus energy has been released the system will again be dominated by the ice albedo feedback. Once the sea ice cover reaches a critical threshold value runaway feedback induced by the ice albedo effect will push the system back to the stadial mode. So if the model were run deterministically the system would either switch to the stadial mode directly after the surplus energy is released from the mid-depth ocean, or not at all. In this case a stochastic perturbation was added to the convergence of the atmospheric heat flux, so that some winters are colder than others. This means that the system can remain in the interstadial mode until during an extremely cold year (or series of cold years) the critical sea ice extent is reached. When this happens the ice albedo effect pushes the system to the fully ice covered state, from which there is no return other than through another DO-event.

A schematic representation of this sequence of events is given in figure 12. The system is bimodal, with a marginally stable interstadial mode, and an initially stable but self destabilizing stadial mode. The right potential well represents the interstadial mode and the deeper left well represents the stadial mode. Panel A represent the situation when the system is its interstadial mode. The system can switch to the stadial mode when the noise in the system pushes it over the potential hill. In this case this involves the sea ice extent crossing a critical threshold during an extremely cold year. When this happens the system becomes fixed in a positive ice albedo feedback loop, which pushes the system towards the fully ice covered state. Once the system is in this state (panel 2) not enough solar energy is absorbed to allow the system to switch back to the interstadial mode. The well is too deep for the noise to be able to tip the system back to interstadial conditions. The only means of exiting the stadial mode is a DO-event. The process of subsurface warming destabilizes the otherwise stable stadial mode and eventually tips the system back to interstadial conditions. After this has happens the surplus energy in the ocean is ventilated rapidly, causing the stadial well to regain its former depth. The system is now back where it started, and the cycle can begin anew.

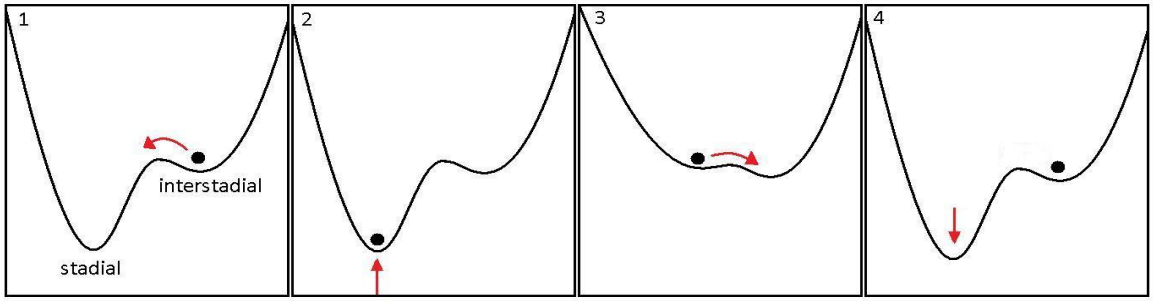

Figure 12, schematic representation of the equilibria of the system. In each panel the left potential well represent the stadial conditions, and the right the interstadial. Moving from left to right shows the sequence of events that forces the system to switch between its equilibira.

When the system is in the interstadial mode it can be pushed over the potential hill into the stadial mode by the noise in the system. The average waiting time before a transition is set by the amplitude of the noise and the depth of the well. The noise represents the year to year variation in atmospheric temperatures, and the depth of the well is to a great extent influenced by the average temperature. The influence of the amplitude of the noise on the interstadial length is investigated in figure 13. In panel A the amplitude of the noise is 5 W/m^2. No transition to stadial conditions is triggered at all during the 10000 years the model is run. Apparently with this noise amplitude winters that are cold enough for the ice cover to pass the critical extent are very rare.

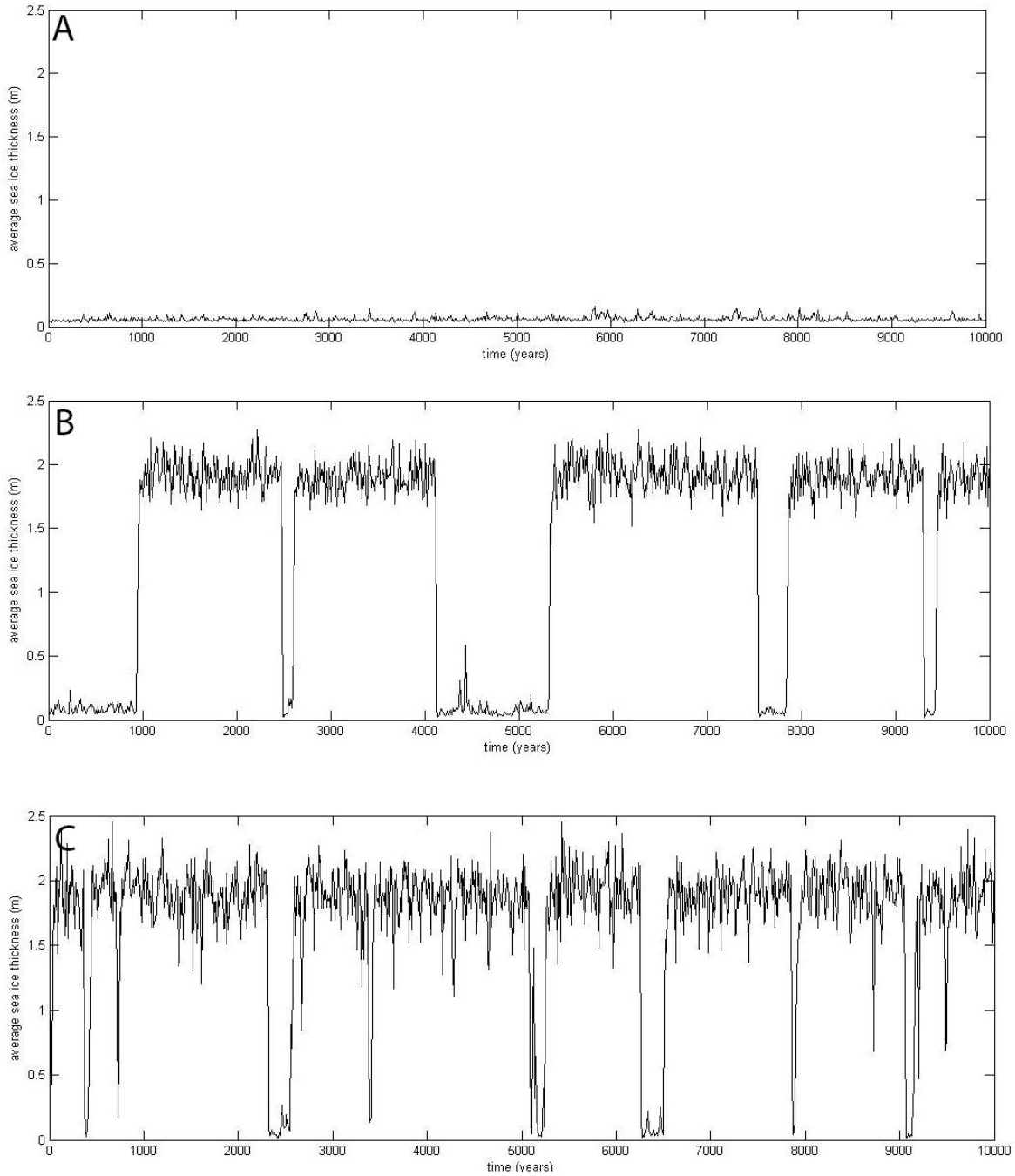

Figure 13, average sea ice thickness plotted vs. time for runs with a different level of noise on the atmospheric temperatures. Panel A; D_{amp} = 5 W/m^2, in B; D_{amp} = 10 W/m^2, and in C; D_{amp} = 15 W/m^2

Panel B shows the results of a model run with a noise amplitude of 10 W/m^2. With this amplitude the chance of crossing the threshold has drastically increased and the bimodality of the system becomes apparent. Addition of symmetric noise has lead to an asymmetric response. The dynamics of the system are altered by the addition of noise, this is referred to as a noise induced transition. The interstadial duration ranges from about 200 to 1000 years. Panel C shows a run with a noise amplitude of 15 W/m^2, another drastic reduction in interstadial duration is observed. Extremely cold winters now occur so frequently that it is impossible for the system to remain in interstadial conditions for longer than a few hundred years.

5.2 Heinrich events

The occurrence of Heinrich events during relatively long stadials indicates that land ice has to be included in the model in order to get a complete picture of the physics driving the DO-cycle. Figure 14 shows the model result for the variables related to the ice shelf over a longer period (15000 years). In panel A the volume of the ice sheet attached to the column model is shown. Under normal conditions the ice sheet has a positive mass balance, so the volume of the sheet increases in time. Around 4500 and 13000 years a surge is triggered, and the discharge of ice into the ocean causes a net mass loss in the sheet. In panel B the shelf extent is plotted, under normal circumstances the shelf covers about 0,5% of the Nordic Seas. The DO-cycle leaves a clear imprint on the shelf extent. To get a better understanding of the variations in the shelf extent the melt rates are plotted in panel C and D. Panel C shows the melt rates relative to the area of shelf (m^3 per m^2 area of shelf), and panel D shows the absolute melt rates (in m^3 normalized with respect to the surface of the column). The melt rates are divided in a top and a bottom melt. In panel C it can be observed that the surface melt (red) is mainly affected by the shifts between the stadial and instadial modes. The melt at the bottom of the shelf closely follows the temperature of the mid-depth ocean (panel B, figure 15). Figure 14 panel D clearly shows that under none surge conditions the total melt rates are quite stable. When the melt rates increase the area of the shelf decreases until the total melt rates are once again in balance with the outflow from the sheet, which is governed by the volume of the ice sheet. The total melt rates increase slowly in time, because the outflow into the shelf also increases due the increasing sheet height.

When the outflow becomes sufficiently large friction is reduced and once this happens the decrease in friction leads to a further increase in the flow speed. It is this positive feedback loop that causes the surging behavior. The decrease in friction means that the total volume flux into in the shelf increases. This causes the shelf to expand and as the area of shelf increases, so do the absolute melt rates. Eventually a new balance is reached, at a much greater shelf extent. As the sheet loses mass the high outflow into the shelf cannot be sustained. This in turn causes a gradual decrease in shelf extent and the absolute melt rates. Furthermore as the outflow decreases this means that at a certain point the friction will start to increase again, terminating the surge. This marks the beginning of a new Heinrich cycle. Surges are more likely to be triggered during stadials, because during these periods the relative melt rates are higher than during interstadials.

In panel A of figure 15 the salinities of the layers are shown and it becomes clear that the surge causes a freshening in the top two layers. (That the mid depth ocean actually becomes slightly saltier is a consequence of how the influx from the Atlantic is calculated. The model is connected to the Stommel model and this uses the average salinity over the whole column to determine the magnitude of the salt influx. As a consequence the freshening of the top two layers leads to an increase in the net salt flux from the Atlantic. As this influx takes place below the halocline the surface layer is not affected by this, but in mid depth ocean layer this increase in the salt influx leads to an increasing salinity.) Once a Heinrich event is triggered the related freshwater input into the surface ocean strengthens the halocline and acts to postpone the instability or DO-event. In panel B it can be observed that the longer duration of the stadial and the stronger halocline cause the subsurface ocean to warm more during the Heinrich stadials than during normal stadials. A feature that has indeed been observed (Ramusssen & Thomson, 2004).

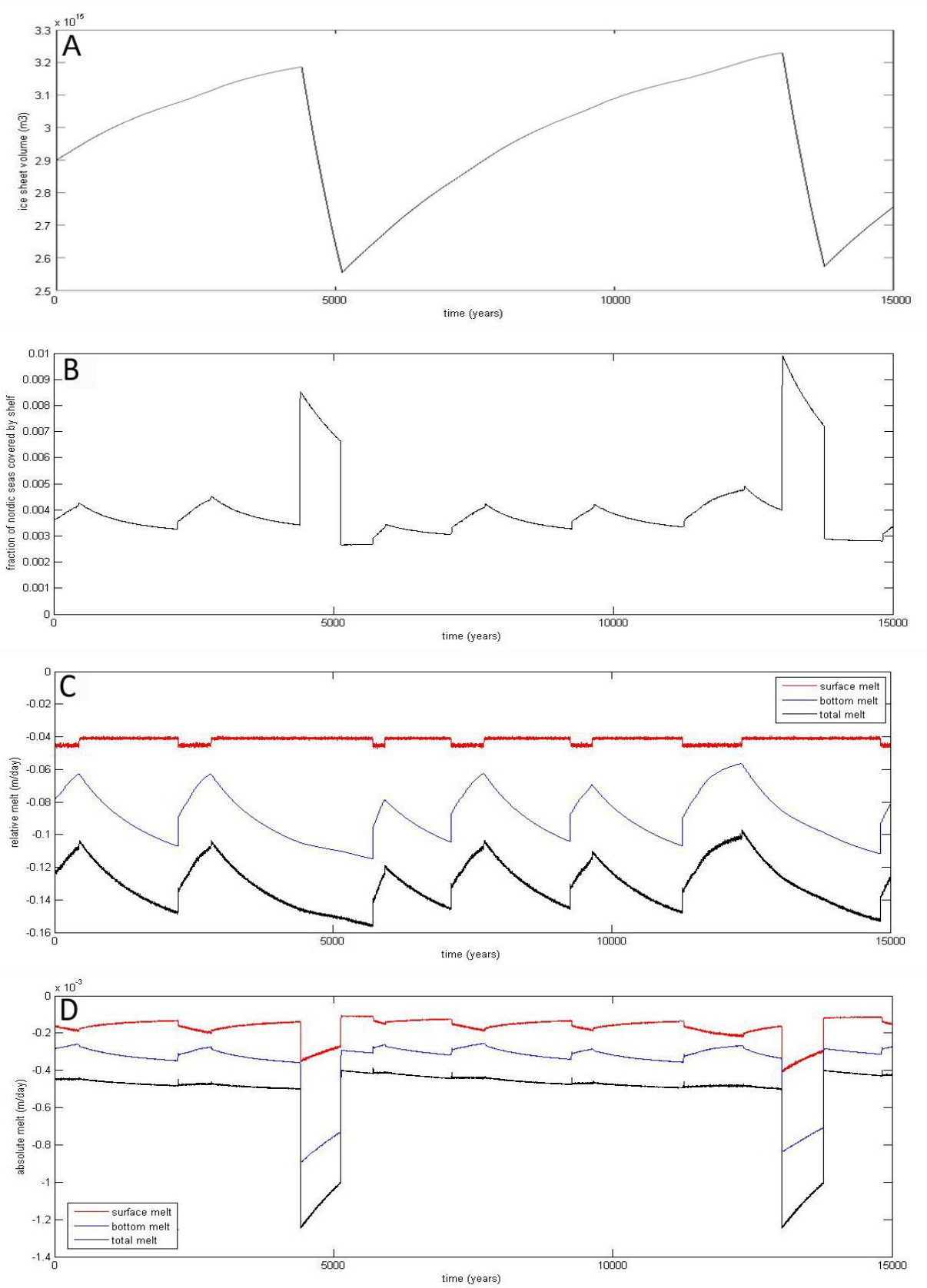

Figure 14, panel A shows the volume of the sheet, panel B the fraction of the Nordic Seas covered by the ice shelf. Panel C&D show the relative and absolute melt rates respectively, red=surface melt, blue=bottom melt, and black=total melt (The first has been normalized with respect to the area of shelf, the second with respect to the surface area of the column).

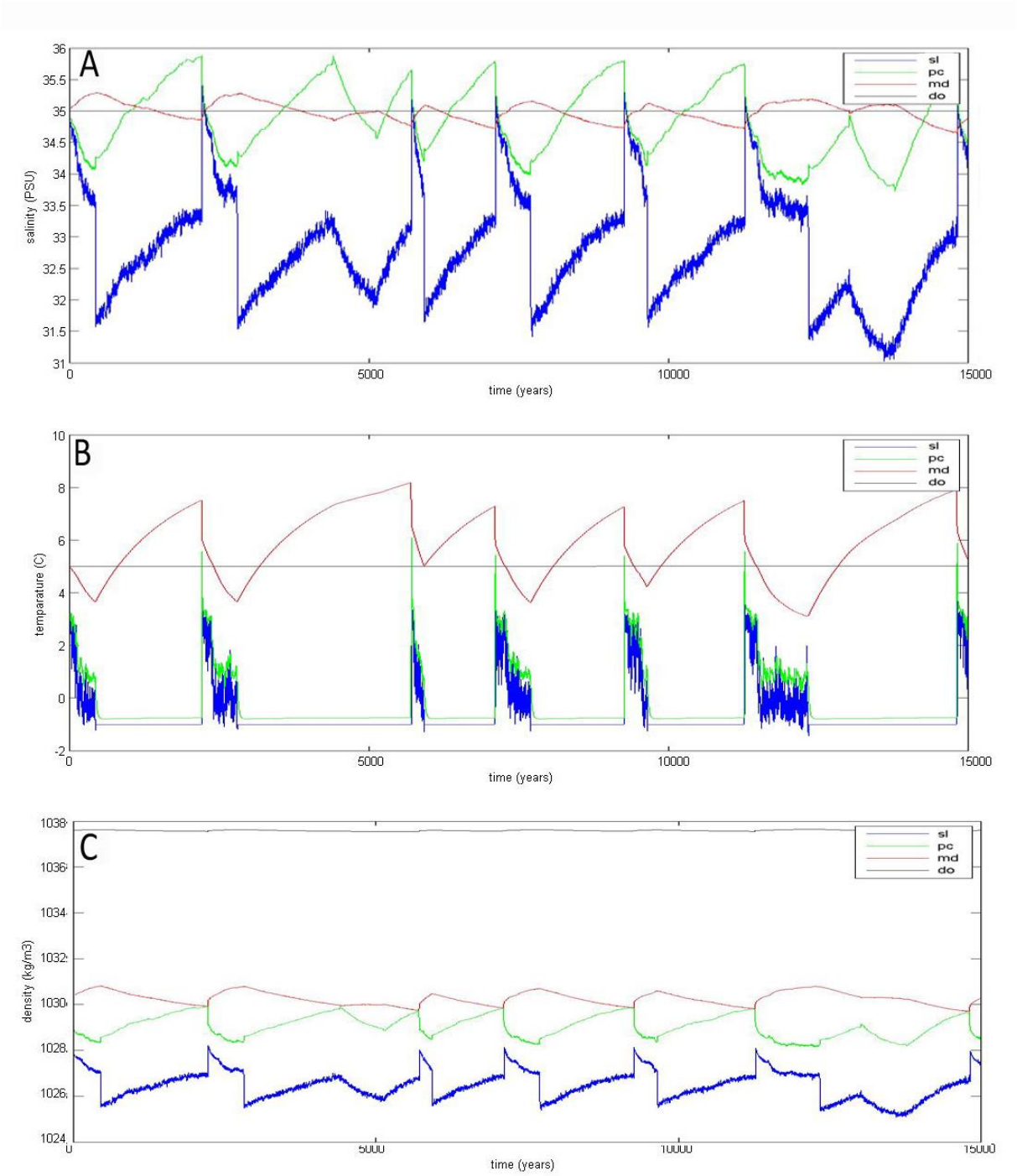

Figure 15, yearly averages salinity (A), temperature (B) and density (C) of the various layers of the column model (sl=surface layer; pc=pycnocline layer; md=middepth ocean layer and do=deep ocean).

5.3 Thermohaline circulation

The main aim of the model was to study the interaction between the temperature changes in the North Atlantic induced by increasing and sea ice cover and the thermohaline circulation. Figure 16 shows strength of the thermohaline circulation calculated from the "Stommel model" for the same

period as figure 14&15. It can be observed that as the stadial progresses and the subsurface waters become warmer, this has a negative effect on the strength of the thermohaline circulation. During the DO-events the subsurface waters lose much of their surplus heat and this cooling leads to an increase in density. The consequence of this increase in density is a sudden increase in the strength of the THC.

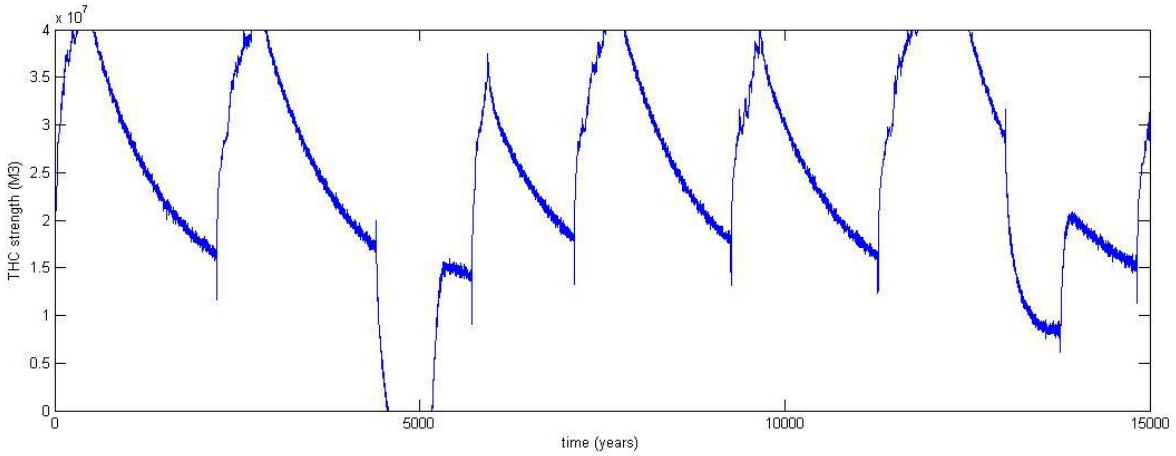

Figure 16. Strength of the thermohaline circulation (in m^3/s) vs. time (in years).

The connection between the AMOC and the DO-events was already apparent (Bond, 1993; EPICA, 2006), and it has been proposed that it were these sudden increases in the AMOC that caused the switch to interstadial conditions. From these results it becomes clear that the relation of cause and effect could be more complex. It is not only the AMOC that drives the climate of the North Atlantic, but the reversed effect might be equally important. During stadial conditions the temperature increase in the subsurface water slows the thermohaline circulation, and this decrease in the energy flux in turn slows the subsurface warming and thus elongates the stadial conditions.

In figure 16 it can be observed that around 5000 years a Heinrich event takes place. The related input of freshwater into the North Atlantic leads to a total shutdown of the THC. In this model a reversal of the THC is inhibited (because in this case if it did happen there would be no mechanism in the model that could get the system out of this mode, it would take the equivalent of a Heinrich event on the Southern hemisphere), but in practice this could occur. That the freshwater flux into the surface ocean associated with the Heinrich event has a direct effect on the waiting time between DO-events has already been discussed. Now it becomes apparent that the Heinrich event also has a secondary effect, namely the shutdown of the THC, which slows the subsurface warming. Close observation of panel B in figure 15 reveals that the rate of warming of the mid depth ocean does indeed decrease. The reason that the subsurface ocean continues to warm even after the THC has been shutdown is the wind driven circulation. After the surge has come to a halt and the salinity anomaly is mixed away by the wind driven circulation, the THC starts up again and the temperature is once again the main controlling factor.

5.4 Air temperature

In the model calculations no explicit air temperature is used, so to compare the model results with the temperature reconstruction from the ice core signal, an air temperature needs to be deduced. To get a simple and effective indication of the air temperature near the surface the fractions of each surface type are simply multiplied by the temperature of that surface:

$$T_{air} = f_{ow}T_{sl} + f_{si}T_{si} + f_{sh}T_{sh} \quad (46)$$

The results are shown in figure 17. The basic structure is quite similar to that of the ice core: A period of rapid warming succeeded by gradual cooling, followed by another sudden jump back to stadial conditions.

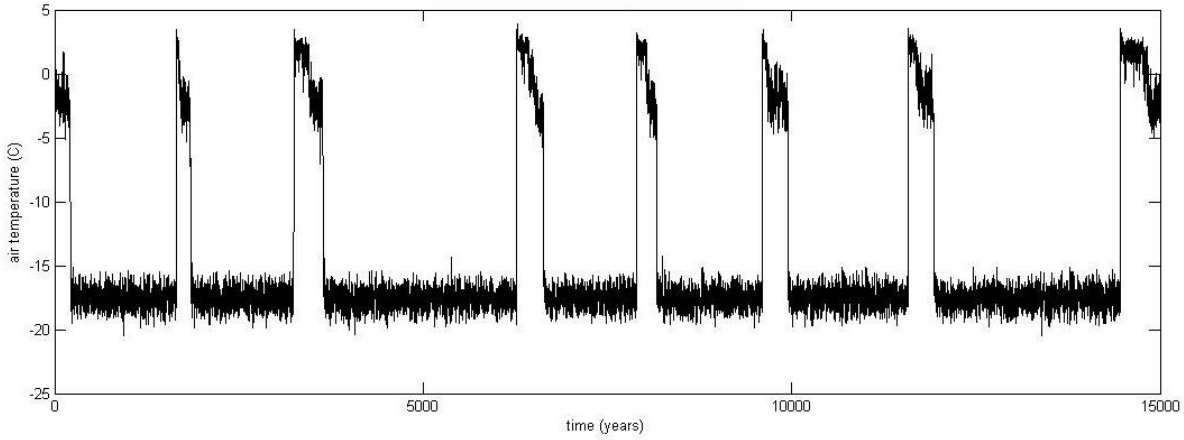

Figure 17, model results for the approximated air temperature near the surface

5.5 Time spacing

The probability density function for the waiting time between DO-events is shown in figure 18. Panel A shows the model results, and panel B the observed waiting times. (note: different scale on x-axis) The ordinary DO-events are shown in blue, and red is used when a Heinrich event occurred during the stadial prior to the DO-event. For the model results the distribution shows a peak around 1500 years, and a secondary peak related to the Heinrich events at 3000 years. These features are also present in the probability distribution based on the ice core signal. The main difference between model results and the observations are the two longest waiting times in the observations.

The first thing to note is that in the observation the spread is much greater for the Heinrich events than in the model results. This can be explained by the fact that due to the simple parameterization of the land ice the freshwater input associated with these events is almost exactly the same for each Heinrich event, whereas in reality this was not the case. If the Heinrich events were parameterized in a more sophisticated fashion which allows for variation in

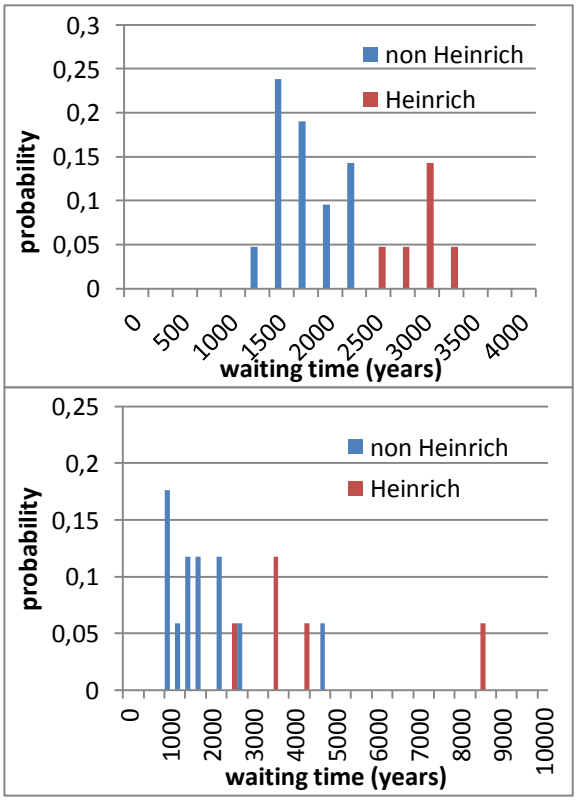

Figure 18, probability density function for the waiting time between consecutive event for the model results (panel A), and the observed events (panel B).

the freshwater flux associated with these events, then this would probably lead to a greater spread in the durations of the waiting times between DO-events. Another thing to note is that all the model parameters are kept constant during the run, whereas in reality there is no reason to assume that they do not change during the ice age. One way of approaching the problem is to think of how changing conditions during the ice age would affect the model parameters and then study how changing these parameters influences the length of the stadials and interstadials. For example the effect of a gradual cooling during the ice age can be studied by varying the average convergence of the atmospheric heat flux over the column D_{ave} while keeping the noise level the same. In figure 19 the effect of varying D_{ave} is shown. Panel A shows the result for slightly colder conditions (-2,5 W/m^2 radiative forcing), and panel B shows a run with slightly warmer conditions (+2,5 W/m^2 radiative forcing). In panel A it can be observed that lower temperatures lead much shorter spiky interstadials. The change in pattern can be explained easily by examining the diagram in figure 12. Colder conditions mean that the right well becomes shallower, and the chances of the noise pushing the system over the potential hill increase drastically. In other words, due to the average colder conditions winters cold enough for the sea ice extent to reach the threshold value are much more common. On the other hand this means that under warmer conditions the stadial length should increase, panel B shows that is indeed the case. In the warm run stadials are much longer, up to 2000 years.

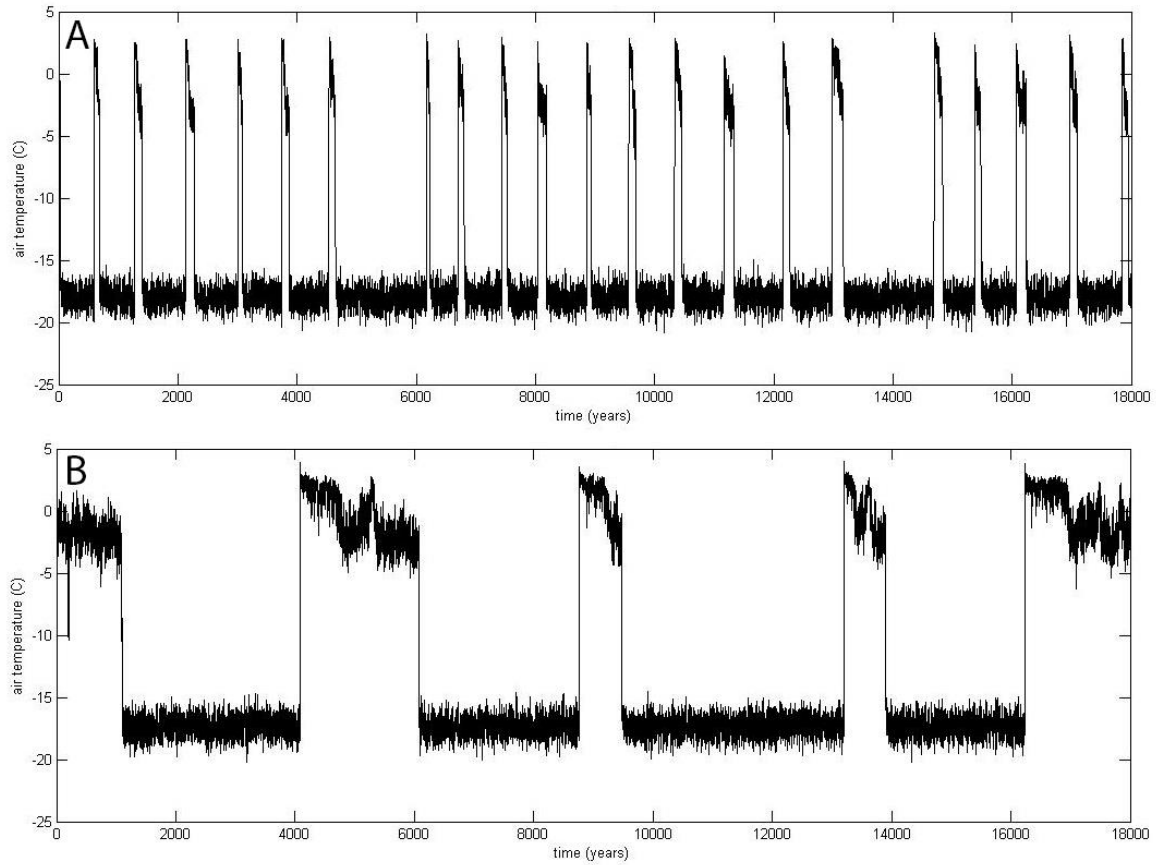

Figure 19, surface temperature vs. time for a model run with D_{ave}=105 W/m^2 (panel A), and D_{ave}=115 W/m^2 (panel B).

Changing the temperature also has an effect on the stadial duration. Although the stadials do seem to have a minimal length, they are much shorter in panel A. The main factor influencing the stadial length is the rate of subsurface warming. As the radiative forcing has only been added to the column (the Southern and Tropical box of the Stommel model do not have an energy balance but an equilibrium temperature), this means that the change in temperature in the northern box is of

influence on the strength of the THC. Colder conditions in the Northern box lead to a stronger circulation, lead to higher rate of subsurface warming. There is also a secondary cause that has to do with salinity. Under colder conditions the average sea ice thickness is greater, this means that every year more sea ice is transported out of the column (fixed percentage of total volume). This export of sea ice can be seen as a negative salt flux out of the column. As noted before this causes the surface ocean to get saltier in time. This means that if more sea ice is transported out of the column this causes the saltening of the surface ocean to proceed more rapidly. This leads to a higher density in the surface ocean and as a consequence the subsurface waters do not need to warm as much for the water column to become unstable, causing the DO-event to occur sooner.

Comparing the results with figure 20 we find that they are in reasonable agreement. In the beginning of the ice age the interstadials are in general much longer (for example after DO-event 19 &20). As the ice age proceeds and the conditions grow colder the interstadials seem to get shorter on average. Near the end of the ice age the DO-events lead only to short spiky interstadials (after DO-event 1-7).

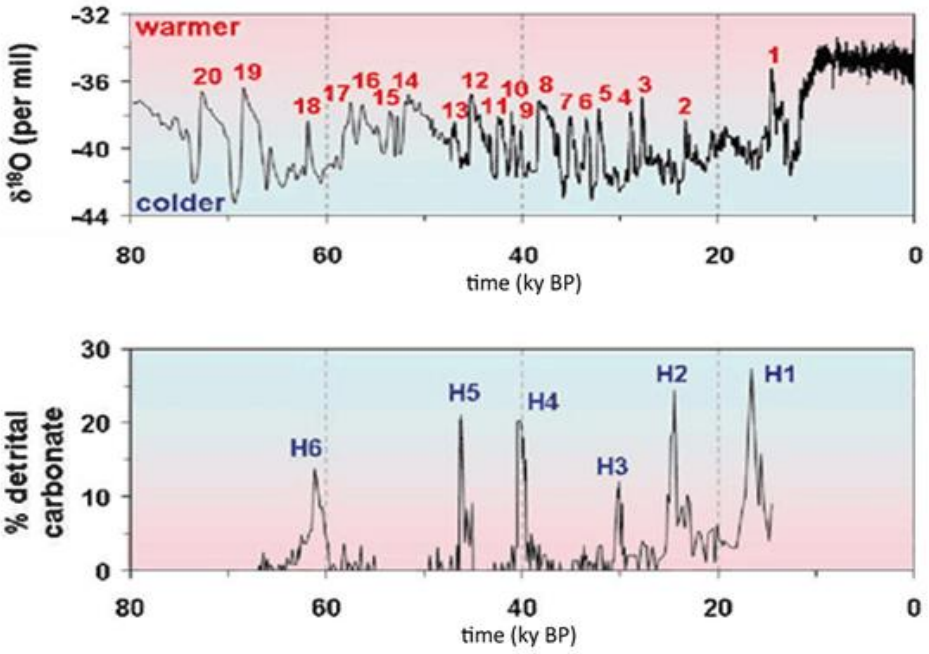

Figure 20, Top: $\delta^{18}O$ from GISP2 ice core, showing 20 of the 25 observed DO-events. (from Grootes et al. 1993) Bottom: A record of ice rafted material from a deep sea core in the North Atlantic. (from Bond and Lotti, 1995)

Another interesting observation is that at the end of the ice age the only DO-events that occur do so directly after Heinrich events. It could be that under the colder conditions the sea has become so thick that ordinary DO-events do not release enough energy to break the ice cover. This would mean that even if instabilities in the water column did occur during this period, they would not be registered as full DO-event in the Greenland isotope signal. However from the model results it became clear that during Heinrich stadials the buildup of energy in the subsurface waters is greater than during normal stadials. If this extra energy proved sufficient to fully melt the sea ice cover, then this could be the reason why only the DO-events following a Heinrich event are registered in the Greenland ice core.

6 Discussion

6.1 Sensitivity

As the model that has been used to test the hypothesis is of a conceptual nature, the question remains open whether the pattern of physical processes that it produces correspond to reality, or whether it is just an artifact of the model formulation. In order to get an impression of how solid the model results are, the sensitivity of the model results to variations in parameters has to be investigated. The sensitivity to the atmospheric forcing has already been analyzed, both for the mean radiative forcing and to the noise level. There are a few other parameters that can significantly influence the results. The other forcing of the model, the shortwave radiation, also plays a crucial role. The manner in which the daily average shortwave radiation is calculated is quite sophisticated, and therein is little room for variation. However the fraction of this ideal amount that actually reaches the earth's surface is variable. Part of it is reflected by clouds, and this amount can vary. In the model this factor is assumed to be constant in time. Varying this parameter will have largely the same effect on the model results as varying the mean convergence of the atmospheric heat flux (D in eq. 11). For example, if less radiation reaches the earth's surface this leads to colder conditions. As a consequence the interstadial mode will become less stable, because winters in which the critical ice extent is reached will occur more frequently. The right potential well in figure 12 will become shallower and therefore the average duration of interstadials will decrease. The main difference between changing the amount of shortwave radiation with respect to changing the longwave radiative forcing, is that the changing the shortwave radiation will have a greater influence on the yearly cycle of the surface temperatures. This is because the shortwave forcing has a yearly cycle, whereas the part of the longwave radiation that is changed (D (eq. 11)) is constant.

The average duration of a stadial is determined by the time it takes for the water column to become unstable. As density is influenced by both temperature and salinity, this time scale is to a great extent influenced by the time evolution of temperature and salinity of the layers involved. This means that there are many parameters that influence the stadial duration. For example, increasing the influx from the Atlantic by increasing the amount of wind driven circulation decreases the stadial duration. This is because an increase in the rate of warming of the subsurface waters leads to a reduction of the time needed before the instability occurs. Whereas increasing the amount of mixing between the surface ocean and the mid-depth ocean would decrease the stadial duration, because this would decrease the rate of warming of the mid-depth ocean.

The evolution of the salinity of the various layers also greatly influences the stadial duration and as a consequence the results are influenced by changes in the mixing coefficients. For example if the amount of mixing between surface layer and the pycnocline layer is increased, then the pycnocline layer will become fresher and therefore lighter. This decrease in density of the pycnocline layer will act to postpone the instability, as the mid-depth ocean will need to warm more before it becomes light enough to lead to instability. Another important parameter is the distribution coefficient of the brine. If more brine is added at greater depth, then the density of the deeper layers will increase with respect to the surface. This will also increase the time necessary for the water column to become unstable. As the sea ice transported out of the column leads a net saltening of the column, this parameter is also of influence on the stadial duration.

Varying these parameters can change the stadial duration from anything from a few decades to thousands of years. However apart from this change in the timescale, the pattern remains largely the same. The periodic instabilities that lead to an energy release are a robust feature of the results. Changing the parameters also influences the profiles of temperature and salinity, this is one further way of checking whether the choice was reasonable. If the profiles in the results are unrealistic, then this is an indication that the timescales might also not be accurate.

For the default values the parameters are all within the realistic range and the profiles of temperature and salinity that they lead to correspond well to observations: The salinity of the fresh surface layer is realistic, and that the thermocline is at greater depth than the halocline is a commonly observed feature. This strengthens the choice of parameters and adds to the plausibility of the hypothesis that these mechanisms act on the timescales seen in the observational data.

6.2 Resolution

For further research it could prove interesting to investigate how increasing the resolution influences the results. The hypothesis depends on the occurrence of a convective mixing event that is the consequence of instability in the water column. The question is whether in reality these events occur on a basin scale, or whether smaller local convective mixing events are favored. When there is but one column representing the entire basin this is of course not an issue, but what happens when the horizontal resolution is increased? Will there be a mechanism that causes a chain reaction so that the instability will occur in many columns almost simultaneously, or at least within a few decades. Or is the opposite more likely, that convective mixing in one column acts to stabilize the surrounding columns. In that case the hypothesis might need to be discarded.

Another way in which increasing the resolution could influence the results is through allowing for a meridional gradient over the basin. In the model this is not the case and this means that when the surface layer cools below freezing, sea ice rapidly forms over the entire basin. If the sea ice extent passes a critical threshold then this quickly leads to total ice cover. Including a meridional temperature gradient in the surface ocean would mean that expansion of sea ice would also involve cooling of the ocean. Whereas in the model in its current form sea ice only forms when the ocean is cold enough, so no further cooling of the ocean is needed for the ice to expand. So including a meridional gradient could make the transitions between the interstadial and stadial mode less rapid, as it would be easier for the system to remain in an in between state for a while.

6.3 Extrapolations

If further research does indeed add to the plausibility of the proposed hypothesis then it might also be interesting to investigate to what extent the mechanism is limited to glacial climate conditions. In theory all that is necessary for the mechanism to work is convergence of the oceanic heat flux below sea ice. But is this really all that is necessary, or can restrictions be formulated for the conditions under which this phenomenon will occur? In other words, how fundamental is this mechanism in keeping the ice-albedo feedback in check?

Another interesting question is how this oscillation on the millennial time scale interacts with the lower frequency variation. As it leads to the energy transported from the equator to the pole being temporarily stored and then released as a “pulse”, this could have a large impact on the average energy that is effectively transported to the northern latitudes. This would mean that integration of this mechanism into models describing low-frequency variation could be important.

7 Conclusions

The model succeeds in providing an explanation for most of the observations related to the DO-cycle. The combination of the mechanisms of AMOC variation, subsurface warming induced by sea ice and a land ice component, has lead to a theory that accounts for the most striking features of the ice core signal and the related observations. This integrated theory can explain more of the data than each of the mechanisms could account for individually, a summary is given in table 1.

Table 1. Summary of the features explained by the individual mechanism and their combination.

Observations:	**AMOC**	**Sea ice**	**Combination**
Greenland temperature	partly	yes	yes
AMOC variation	yes	no	yes
Subsurface warming Nordic Seas	no	yes	yes
Heinrich events			
-delaying DO-event	yes	yes	yes
-triggered during stadials	no	yes	yes
-weakening of AMOC before events	no	no	yes
-Bond cycle	partly	no	partly
Wetter warmer Europe during interstadials	yes	yes	yes

The conceptual model provides an explanation for the structure of the DO-events, the timescales involved and the variation therein. It explains the change in interstadial duration as the ice age progresses and accounts for most of the variability in the stadial duration. It shows why the relatively long stadials occur during Heinrich events and why these events are counter intuitively triggered during stadials. Furthermore the inclusion of the Heinrich events leads to an alternative explanation to stochastic resonance for the double peak in the probability distribution of the waiting time between consecutive events. What the model does not account for is how an ice discharge from the Scandinavian ice sheet leads to an instability in the Laurentide ice sheet, although the occurrence of these precursor events is in agreement with observations (Alvarez Solas, 2011). Ocean temperature reconstructions show warming during stadials above the Iceland- Scotland ridge (Rasmussen& Thompsen, 2004; Dokken, 2013) and cooling south of it (Bond, 1993), this pattern is successfully explained.

The model results might agree well with much of the observational data, however the model is not elaborate enough to provide conclusive answers. Support from further research with more sophisticated means would greatly add to the credibility of the hypothesis.

Appendix 1

Parameters	Symbol	Value	Unit	Description
Forcing:	D_{mean}	10	W/m^2	Convergence of atmospheric heat flux.
	D_{amp}	110	W/m^2	Amplitude of noise.
	C_{cloud}	0,25	-	Fraction of S_{in} reflected by clouds
Spatial dimensions:	A_n	10^{12}	m^2	Surface of column
	A_{sheet}	10^{12}	m^2	Surface of ice sheet
	h_{sl}	40	m	Thickness of surface layer
	h_{pc}	360	m	Thickness of pycnocline layer
	h_{md}	1600	m	Thickness of mid-depth ocean layer
	h_{do}	2000	M	Thickness of deep ocean layer
	h_{si}^0	0,5	M	Initial sea ice thickness
	h_{shelf}	400	M	Thickness of ice shelf
	V_s	$1{,}1\cdot10^{17}$	m^3	Volume of southern box
	V_t	$0{,}68\cdot10^{17}$	m^3	Volume of tropical box
	V_d	$0{,}05\cdot10^{17}$	m^3	Volume of deep box
	z_s	3000	M	Thickness of southern box
	z_t	1000	M	Thickness of tropical box
Stommel model:	K	$25{,}4\cdot10^{17}$	m^3/y	Hydrolic coefficient
	r	$7{,}3\cdot10^{8}$	$J/y/m^2/K$	Thermal coupling constant
	T_s^{eq}	279	K	Equilibrium temperature southern box
	T_t^{eq}	293	K	Equilibrium temperature tropical box
	F_s	0,014	Sv	Southward atmospheric moisture flux
	F_n	0,024	Sv	Northward atmospheric moisture flux
	C_{wn}	100	Sv	Volume transported by the Gulfstream
Flux-gradient Coefficients:	KT_{sl-pc}^{wat}	$5\cdot10^{-4}$	m^2/s	Mixing coefficients (from Singh(2013))
	KT_{sl-pc}^{ice}	$1\cdot10^{-4}$	m^2/s	
	KT_{md-pc}	$1\cdot10^{-5}$	m^2/s	
	KT_{do-md}	$1\cdot10^{-7}$	m^2/s	
	KS_{sl-pc}^{wat}	$5\cdot10^{-4}$	m^2/s	
	KS_{sl-pc}^{ice}	$1\cdot10^{-4}$	m^2/s	
	KS_{md-pc}	$1\cdot10^{-5}$	m^2/s	
	KS_{do-md}	$1\cdot10^{-8}$	m^2/s	
	C_{tur}	20	$W/m^2/K$	Turbulent exchange coefficient
	$C_{sl\text{-}si}$	20	$W/m^2/K$	Flux-gradient coefficient sea ice bottom
	$C_{sl\text{-}sh}$	40	$W/m^2/K$	Flux-gradient coefficient shelf bottom
Distribution coefficients:	J_{sl}	0,05	-	Distribution coefficients determining the distribution of the inflow from the Atlantic over the various layers.
	J_{pc}	0,20	-	
	J_{md}	0,75	-	
	B_{sl}	0	-	Distribution coefficients determining the distribution of the brine formed during sea ice formation.
	B_{pc}	0,75	-	
	B_{md}	0,25	-	
Export coefficients	C_x	25	-	Percentage of sea ice exported annually
	C_x^{sh}	3	-	Link between melt and ice berg export
Land ice parameters	τ_f	0,05	$year^{-1}$	Relates flow speed to extent deficit
	C_s	1-2,5	-	Stream coefficient
	R_{min}	$5\cdot10^{-3}$	-	Ratio between volumes of sheet and shelf
	P_p	0,9	-	Fraction of moisture flux added to sheet

Constants	Value	Unit	Description
c_p	3850	J/kg/K	Specific heat of sea water
c_p^{ice}	2050	J/kg/K	Specific heat of ice
L_f	334000	J/kg	Latent heat of fusion
$\boldsymbol{\rho}_0$	1025	kg/m^3	Reference density
$\boldsymbol{\rho}_{ice}$	900	kg/m^3	Density of ice
S_0	35	PSU	Reference salinity
T_0	-1,8	°C	Freezing temperature
α_w	0,1	-	Albedo of water
α_{ice}	0,75	-	Albedo of sea ice
α_{shelf}	0,6	-	Albedo of ice shelf
A	320	W/m^2	Constants for linearization of Boltzmann's law
B	4,6	W/m^2/K	

References

Aagaard, K., L. K. Coachman, and E. armack, On the halocline of the Arctic Ocean, Deep Sea Res., Part A, 28, 529-545, 1981.

Álvarez-Solas, Jorge, et al. "Heinrich event 1: an example of dynamical ice-sheet reaction to oceanic changes." Climate of the Past 7 (2011): 1297-1306.

Arbic, B., MacAyeal, D., Mitrovica, J., and Milne, G.: PalaeoclimateOcean tides and Heinrich events, Nature, 432, 460–460, 2004. 1569

Berger, A. "k Loutre, MF 1991 Insolation values for the climate of the last 10 my Quat. Sci. Rev. 10, 297-317." Berger29710Quat. Sci. Rev (1991).

Bond, Gerard, et al. "Correlations between climate records from North Atlantic sediments and Greenland ice." Nature 365.6442 (1993): 143-147.

Bond, Gerard C., and Rusty Lotti. "Iceberg discharges into the North Atlantic on millennial time scales during the last glaciation." Science 267.5200 (1995): 1005-1010.

Braun, H., et al. "A two-parameter stochastic process for Dansgaard-Oeschger events." Paleoceanography 26.3 (2011).

Broecker, Wallace S., et al. "A salt oscillator in the glacial Atlantic? 1. The concept." Paleoceanography 5.4 (1990): 469-477.

Broecker, Wallace S. "Paleocean circulation during the last deglaciation: a bipolar seesaw?." Paleoceanography 13.2 (1998): 119-121.

Calov, Reinhard, et al. "Large-scale instabilities of the Laurentide ice sheet simulated in a fully coupled climate-system model." Geophysical Research Letters 29.24 (2002): 69-1.

Cimatoribus, A. A., et al. "Dansgaard–Oeschger events: bifurcation points in the climate system." Climate of the Past 9.1 (2013): 323-333.

Crowley, T. J. (1992), North Atlantic deep water cools the Southern Hemisphere, Paleoceanography, 7, 489–497.

Dansgaard, Willi, et al. "Evidence for general instability of past climate from a 250-kyr ice-core record." Nature 364.6434 (1993): 218-220.

Dansgaard, W., S. J. Johnson, H. B. Clausen, D. Dahl-Jensen, N. Hammer, and C. U. Oeschger, 1984: North Atlantic climatic oscillations revealed by deep greenland ice cores. Climate Processes and Climate Sensitivity, Geophys. Monogr., No. 29, Amer.Geophys. Union, 288–298.

Delworth, Thomas L., and Fanrong Zeng. "Simulated impact of altered Southern Hemisphere winds on the Atlantic meridional overturning circulation." Geophysical Research Letters 35.20 (2008).

Ditlevsen, Peter D., and Sigfus J. Johnsen. "Tipping points: early warning and wishful thinking." Geophysical Research Letters 37.19 (2010).

Ditlevsen, Peter D., Katrine K. Andersen, and Anders Svensson. "The DO-climate events are probably noise induced: statistical investigation of the claimed 1470 years cycle." Climate of the Past 3.1 (2007): 129-134.

Dokken, Trond M., et al. "Dansgaard-Oeschger cycles: Interactions between ocean and sea ice intrinsic to the Nordic seas." Paleoceanography 28.3 (2013): 491-502.

EPICA community members. "One-to-one coupling of glacial climate variability in Greenland and Antarctica." Nature 444.7116 (2006): 195-198.

Fleitmann, D., et al. "Timing and climatic impact of Greenland interstadials recorded in stalagmites from northern Turkey." Geophysical Research Letters 36.19 (2009).

Ganopolski, Andrey, and Stefan Rahmstorf. "Rapid changes of glacial climate simulated in a coupled climate model." Nature 409.6817 (2001): 153-158.

Garcin, Yannick, et al. "Wet phases in tropical southern Africa during the last glacial period." Geophysical Research Letters 33.7 (2006).

Genty, Dominique, et al. "Precise dating of Dansgaard–Oeschger climate oscillations in western Europe from stalagmite data." Nature 421.6925 (2003): 833-837.

Gildor, Hezi, and Eli Tziperman. "A sea ice climate switch mechanism for the 100-kyr glacial cycles." Journal of Geophysical Research: Oceans (1978–2012) 106.C5 (2001): 9117-9133.

Grootes, P. M., and M. Stuiver. "Oxygen 18/16 variability in Greenland snow and ice with 10− 3-to 105-year time resolution." Journal of Geophysical Research: Oceans (1978–2012) 102.C12 (1997): 26455-26470.

Grootes, P.M., Stuiver, M., White, J.W.C., Johnsen, S.J. and Jouzel, J. 1993. Comparison of oxygen isotope records from the GISP2 and GRIP Greenland ice cores. Nature 366: 552-554.

Hall, I. R., Moran, S. B., Zahn, R., Knutz, P. C., Shen, C. C., and Edwards, R. L.: Accelerated drawdown of meridional overturning in the late-glacial Atlantic triggered by transient pre-H event freshwater perturbation, Geophys. Res. Lett., 33, L16616,doi:10.1029/2006GL026239, 2006. 1568, 1569, 1574;

Harrison, S. P., and M. F. Sanchez Goñi. "Global patterns of vegetation response to millennial-scale variability and rapid climate change during the last glacial period." Quaternary Science Reviews 29.21 (2010): 2957-2980.

Heinrich, Hartmut. "Origin and consequences of cyclic ice rafting in the northeast Atlantic Ocean during the past 130,000 years." Quaternary research 29.2 (1988): 142-152.

Held, H. and T. Kleinen. "Detection of climate system bifurcations by degenerate fingerprinting." Geophysical Research Letters 31.23 (2004).

Hemming, Sidney R. "Heinrich events: Massive late Pleistocene detritus layers of the North Atlantic and their global climate imprint." Reviews of Geophysics 42.1 (2004).

Hulbe, C. L., et al. "Catastrophic ice shelf breakup as the source of Heinrich event icebergs." Paleoceanography 19.1 (2004).

Hulbe, C. "Palaeoclimate: Extreme iceberg generation exposed." Nature Geoscience 3.2 (2010): 80-81.

Johnsen, S. J., et al. "Irregular glacial interstadials recorded in a new Greenland ice core." Nature 359.6393 (1992): 311-313.

Knutti, R., et al. "Strong hemispheric coupling of glacial climate through freshwater discharge and ocean circulation." Nature 430.7002 (2004): 851-856.

Kreveld, S. van, et al. "Potential links between surging ice sheets, circulation changes, and the Dansgaard-Oeschger Cycles in the Irminger Sea, 60–18 Kyr." Paleoceanography 15.4 (2000): 425-442.

Levermann, Anders, et al. "Dynamic sea level changes following changes in the thermohaline circulation." Climate Dynamics 24.4 (2005): 347-354.

Li, Camille, et al. "Abrupt climate shifts in Greenland due to displacements of the sea ice edge." Geophysical Research Letters 32.19 (2005).

Livina, Valerie N., and Timothy M. Lenton. "A modified method for detecting incipient bifurcations in a dynamical system." Geophysical Research Letters 34.3 (2007).

MacAyeal, D. R. "Binge/purge oscillations of the Laurentide ice sheet as a cause of the North Atlantic's Heinrich events." Paleoceanography 8.6 (1993): 775-784.

Menviel, L., et al. "Hindcasting the continuum of Dansgaard–Oeschger variability: mechanisms, patterns and timing." Climate of the Past 10.1 (2014): 63-77.

Mignot, J., Ganopolski, A., and Levermann, A.: Atlantic subsurface temperatures: response to a shut-down of the overturning circulation and consequences for its recovery, J. Clim., 20, 4884–4898, 2007. 1569

Pausata, Francesco SR, et al. "Chinese stalagmite [delta] 18O controlled by changes in the Indian monsoon during a simulated Heinrich event." Nature Geoscience 4.7 (2011): 474-480.

*Rahmstorf, Stefan, Matthew H. England, 1997: Influence of Southern Hemisphere Winds on North Atlantic Deep Water Flow. J. Phys. Oceanogr., **27**, 2040–2054.*

Rahmstorf, Stefan. "Ocean circulation and climate during the past 120,000 years." Nature 419.6903 (2002): 207-214.

Rasmussen, Tine L., and Erik Thomsen. "The role of the North Atlantic Drift in the millennial timescale glacial climate fluctuations." Palaeogeography, Palaeoclimatology, Palaeoecology 210.1 (2004): 101-116.

Sakai, K., and W. R. Peltier. "A simple model of the Atlantic thermohaline circulation: Internal and forced variability with paleoclimatological implications." Journal of Geophysical Research: Oceans (1978–2012) 100.C7 (1995): 13455-13479.

Sarnthein, M. et al. Changes in east Atlantic deepwater circulation over the last 30,000 years: Eight time slice reconstructions. Paleoceanography 9, 209±267 (1994).

Scheffer, Marten, et al. "Early-warning signals for critical transitions." Nature 461.7260 (2009): 53-59.

Schulz, Michael. "On the 1470-year pacing of Dansgaard-Oeschger warm events." Paleoceanography 17.2 (2002): 4-1.

Schulz, Hartmut, et al. "Correlation between Arabian Sea and Greenland climate oscillations of the past 110,000 years." Nature 393.6680 (1998): 54-57.

Shaffer, G., Olsen, S., and Bjerrum, C.: Ocean subsurface warming as a mechanism for coupling Dansgaard-Oeschger climate cycles and ice-rafting events, Geophys. Res. Lett., 31, L24202, doi:10.1029/2004GL020968, 2004. 1570, 1574

Singh, Hansi A., David S. Battisti, and Cecilia M. Bitz. "A Heuristic Model of the Dansgaard-Oeschger Cycles: Description, Results, and Sensitivity Studies: Part I." Journal of Climate 2013 (2013).

Spötl, Christoph, and Augusto Mangini. "Stalagmite from the Austrian Alps reveals Dansgaard–Oeschger events during isotope stage 3:: Implications for the absolute chronology of Greenland ice cores." Earth and Planetary Science Letters 203.1 (2002): 507-518.

Stocker, Thomas F., and Sigfùs J. Johnsen. "A minimum thermodynamic model for the bipolar seesaw." Paleoceanography 18.4 (2003).

Stommel H (1961) Thermohaline convection with two stable regimes of flow. Tellus 13: 224–241

Timmermann, Axel, et al. "Coherent resonant millennial-scale climate oscillations triggered by massive meltwater pulses." Journal of Climate 16.15 (2003): 2569-2585.

Toggweiler, J. R., and B. Samuels. "Is the magnitude of the deep outflow from the Atlantic Ocean actually governed by Southern Hemisphere winds?." The Global Carbon Cycle. Springer Berlin Heidelberg, 1993. 303-331.

Voelker, Antje HL. "Global distribution of centennial-scale records for Marine Isotope Stage (MIS) 3: a database." Quaternary Science Reviews 21.10 (2002): 1185-1212.

Wagner, J. D. M., et al. "Moisture variability in the southwestern United States linked to abrupt glacial climate change." Nature Geoscience 3.2 (2010): 110-113.

Wang, Yong-Jin, et al. "A high-resolution absolute-dated late Pleistocene monsoon record from Hulu Cave, China." Science 294.5550 (2001): 2345-2348.

Hughes, Tertia MC, and Andrew J. Weaver. "Multiple equilibria of an asymmetric two-basin ocean model." Journal of Physical Oceanography 24.3 (1994): 619-637.

Winton, Michael, and E. S. Sarachik. "Thermohaline oscillations induced by strong steady salinity forcing of ocean general circulation models." Journal of Physical Oceanography 23.7 (1993): 1389-1410.

Zickfeld, Kirsten, Thomas Slawig, and Stefan Rahmstorf. "A low-order model for the response of the Atlantic thermohaline circulation to climate change." Ocean Dynamics 54.1 (2004): 8-26.